

Superspace calculation of the four-loop spectrum in $\mathcal{N} = 6$ supersymmetric Chern-Simons theories

M. Leoni ^{a,b}, A. Mauri ^{a,b}, J. A. Minahan ^c, O. Ohlsson Sax ^c,
A. Santambrogio ^b, C. Sieg ^{d,e}, G. Tartaglino-Mazzucchelli ^{c*}

^a *Dipartimento di Fisica, Università degli Studi di Milano
Via Celoria 16, 20133 Milano, Italy*

^b *INFN-Sezione di Milano
Via Celoria 16, 20133 Milano, Italy*

^c *Department of Physics and Astronomy, Uppsala University
SE-751 08 Uppsala, Sweden*

^d *The Niels Bohr International Academy
The Niels Bohr Institute
Blegdamsvej 17, 2100 Copenhagen, Denmark*

^e *Institute für Mathematik/Physik, Humboldt-Universität zu Berlin
Rudower Chaussee 25, 12489 Berlin, Germany*

Abstract

Using $\mathcal{N} = 2$ superspace techniques we compute the four-loop spectrum of single trace operators in the $SU(2) \times SU(2)$ sector of ABJM and ABJ supersymmetric Chern-Simons theories. Our computation yields a four-loop contribution to the function $h^2(\lambda)$ (and its ABJ generalization) in the magnon dispersion relation which has fixed maximum transcendentality and coincides with the findings in components given in the revised versions of arXiv:0908.2463 and arXiv:0912.3460. We also discuss possible scenarios for an all-loop function $h^2(\lambda)$ that interpolates between weak and strong couplings.

*matias.leoni@mi.infn.it,
andrea.mauri@mi.infn.it,
joseph.minahan@fysast.uu.se,
olof.ohlsson-sax@physics.uu.se,
alberto.santambrogio@mi.infn.it,
csieg@nbi.dk, csieg@math.hu-berlin.de
gabriele.tartaglino-mazzucchelli@fysast.uu.se

1 Introduction

The ABJM model is an $\mathcal{N} = 6$ supersymmetric $U(N) \times U(N)$ Chern-Simons theory with opposite levels coupled to matter [1]. Like its cousin $\mathcal{N} = 4$ super Yang-Mills in four dimensions, its two point functions of single trace operators map to an integrable system in the planar limit [2–5]. For $\mathcal{N} = 4$ SYM, the integrability has been used as a powerful tool to interpolate between strong and weak coupling, where one can see the perturbative behavior of the gauge theory morph into the stringy behavior expected from the AdS/CFT conjecture [6, 7].

The ABJM model has two extra features that give it a richer structure than $\mathcal{N} = 4$ SYM, at least as far as the integrability of the two point functions is concerned. The first is that the Bethe equations and the dispersion relations contain an undetermined function $h^2(\lambda)$ of the 't Hooft coupling, $\lambda = N/k$, where k is the Chern-Simons level [5]. The second is that the theory can be deformed into a $U(M) \times U(N)$ gauge theory while still maintaining the $\mathcal{N} = 6$ supersymmetry [8]. In this ABJ case there are now two 't Hooft parameters,

$$\lambda = \frac{M}{k}, \quad \hat{\lambda} = \frac{N}{k}, \quad (1.1)$$

and, if integrability is maintained, a single function $h^2(\bar{\lambda}, \sigma)$, where

$$\bar{\lambda} = \sqrt{\lambda \hat{\lambda}}, \quad \sigma = \frac{\lambda - \hat{\lambda}}{\lambda}. \quad (1.2)$$

The spin-chain that appears in the ABJ(M) models has $OSp(6|4)$ symmetry and is of alternating type, with the spins on the odd sites in the singleton representation of the supergroup and the spins on the even sites in the anti-singleton representation [2–4, 9, 10]. In order to find $h^2(\bar{\lambda}, \sigma)$ it is only necessary to consider the compact subgroup $SU(2) \times SU(2)$ of $OSp(6|4)$, with the spins on the odd sites transforming in the $(\mathbf{2}, \mathbf{1})$ representation and the spins on the even sites transforming in the $(\mathbf{1}, \mathbf{2})$ representation. The ground state has all spins aligned and the excitations (or magnons) are flipped spins that live on either odd or even sites. The dispersion relations for these two types of magnons are given by

$$E_{\text{odd}}(p) = \sqrt{Q^2 + 4h^2(\bar{\lambda}, \sigma) \sin^2 \frac{p}{2}} - Q, \quad E_{\text{even}}(p) = E_{\text{odd}}(p)|_{\sigma \rightarrow -\sigma}, \quad (1.3)$$

where $Q = 1/2$ for fundamental magnons while larger values of Q correspond to magnon bound states.

At weak coupling the function $h^2(\bar{\lambda}, \sigma)$ can be computed perturbatively. The leading contribution appears at two-loop order and is relatively easy to compute, both for ABJM [2–4], and ABJ [10, 11], where one finds

$$h^2(\bar{\lambda}, \sigma) = \bar{\lambda}^2 + \mathcal{O}(\bar{\lambda}^4). \quad (1.4)$$

However, at strong coupling on the ABJM slice where $\sigma = 0$, one readily finds from the string sigma model [3, 12, 13].

$$h^2(\bar{\lambda}, 0) = \frac{1}{2} \bar{\lambda} + \mathcal{O}(1). \quad (1.5)$$

Hence, $h^2(\bar{\lambda}, \sigma)$ is an interpolating function and can be expected to have corrections at every even order of perturbation theory, with a general structure

$$h^2(\bar{\lambda}, \sigma) = \bar{\lambda}^2 + \sum_{n=2}^{\infty} \bar{\lambda}^{2n} h_{2n}(\sigma) . \quad (1.6)$$

The four-loop term in (1.6) was computed in [14, 15], where it was found that¹

$$h_4(\sigma) = -(4 + \sigma^2)\zeta(2) . \quad (1.7)$$

This calculation was done using the explicit component action and involved the computation of dozens of Feynman diagrams. A straightforward extension of the methods in [14, 15] to higher loops would lead to a mind boggling number of diagrams. Moreover, one would like to verify (or disprove) that the ABJ theory is integrable, even at the four-loop order. The $SU(2) \times SU(2)$ sector is trivially integrable at four loops, so it would be necessary to go beyond this sector to find a nontrivial check of integrability at this order. But even this seemingly modest task is extremely daunting in component language.

In this paper we compute $h_4(\sigma)$ in (1.7) using the superspace formalism. Superspace techniques have proven to be very effective in computing the dilatation operator [16] and in evaluating wrapping corrections [17, 18] in $\mathcal{N} = 4$ SYM [19, 20] and in its β -deformation [21–23]. Naturally, one would also like to apply them to the ABJ(M) models. Their main virtue is that they drastically reduce the number of Feynman diagrams that one must compute. We will later summarize several restrictions on the allowed diagrams [16] that greatly limit the number that can contribute to $h_4(\sigma)$. As we will see in this paper, at the two-loop order there is only one diagram in superspace that contributes to $h^2(\bar{\lambda}, \sigma)$. At the four-loop order there are 15 (plus reflections of some of the diagrams). Contrast this to the component calculation in [14, 15], where one has many times more diagrams. Not only does this demonstrate the formalism’s power, but it is also crucial in verifying that (1.7) is actually correct (see footnote 1).

One can also see from (1.7) that $h_4(\sigma)$ has uniform transcendentality two. From the component point of view this seems almost miraculous since many diagrams have rational coefficients (that is, they have transcendentality zero), others have transcendentality two, and some are mixed. When everything is combined one finds that the rational coefficients cancel. In superspace, while there are still diagrams with rational coefficients, their cancellation appears more natural due to correlations between the single and double poles.

We will also present two possible scenarios for an all-loop function for $h^2(\lambda)$, including one that might work. It reproduces the first two orders of perturbation theory as well as the leading sigma-model contribution at strong-coupling. The one-loop sigma-model contribution to $h^2(\lambda)$ depends on how a sum is carried out over an infinite number of modes. Our proposal disagrees with the more conventional prescription in [24], but agrees with the prescription in [25]. The other proposal looks for a connection with

¹A different result for $h_4(\sigma)$ in (1.7) was given in earlier versions of [14, 15]. After it became clear that those results were in conflict with the results presented in this paper, an overall sign error was discovered for three of the Feynman graphs.

matrix models on a Lens space. These arise in the study of supersymmetric Wilson loops in ABJ(M) models [26–29]. In particular, we consider the free energy of the matrix model which is a function of λ . We will see that $h^2(\lambda)$ has a structure similar to the derivative of the matrix model free energy, both at small and large λ . But the coefficients in their respective expansions do not quite line up.

In order to complete the four-loop analysis in the $SU(2) \times SU(2)$ subsector, we will apply the superspace formalism to compute the leading wrapping corrections for a length four operator in the $(\mathbf{1}, \mathbf{1})$ representation of $SU(2) \times SU(2)$. Here we find that the wrapping corrections *per se* differ from those computed in component language. However, other range five interactions must be subtracted and this subtracted piece also differs from the corresponding term in the component calculation. The two effects combine to give the same four-loop anomalous dimension for this operator as was found using components.

The rest of the paper is organized as follows: In section 2 we review the ABJ(M) models in $\mathcal{N} = 2$ superspace. In section 3 we discuss the relation of the dilatation operator to $h^2(\bar{\lambda}, \sigma)$. In section 4 we enumerate and compute all Feynman diagrams that contribute to the four-loop term $h_4(\sigma)$. In section 5 we discuss our investigation into possible all-loop functions for $h^2(\lambda)$. In section 6 we apply the superspace formalism to the wrapping corrections for operators of length four. In section 7 we present our conclusions, which includes suggestions for further work. Many further details, including the four-loop decoupling of odd and even site magnons and the consistency of double poles due to UV subdivergences can be found in the several appendices.

2 ABJ(M) models in $\mathcal{N} = 2$ superspace

In this section we review the $\mathcal{N} = 2$ superspace formulation for $\mathcal{N} = 6$ superconformal Chern-Simons theory. This was first given in [30], but in this paper we follow the notations used in [31] which are adapted from the ones of [32]. For the first papers on the $\mathcal{N} = 2$ superspace formulation of Chern-Simons theory coupled to matter see [33–36]. Appendix A collects our notation and conventions.

The $U(M) \times U(N)$ supersymmetric Chern-Simons theory has two $\mathcal{N} = 2$ vector supermultiplets, V and \hat{V} , with V transforming in the adjoint of $U(M)$ and \hat{V} in the adjoint of $U(N)$. In order to extend the supersymmetry to $\mathcal{N} = 6$, the ABJ(M) action also contains two sets of chiral matter superfields, Z^A and W_A with $A = 1, 2$. Z^A and W_A transform respectively in the $(\mathbf{2}, \mathbf{1})$ and $(\mathbf{1}, \mathbf{2})$ of the global $SU(2) \times SU(2)$ flavour subgroup described in the introduction. Moreover, they transform in the bifundamental representations $(\mathbf{M}, \bar{\mathbf{N}})$ and $(\mathbf{N}, \bar{\mathbf{M}})$ of the $U(M) \times U(N)$ gauge group.

Each gauge group in the gauge fixed $\mathcal{N} = 2$ superspace action has associated with it a pair of chiral ghost superfields, c, c' for $U(M)$ and \hat{c}, \hat{c}' for $U(N)$ [37–39]. Including

all of these ingredients, the gauge fixed ABJ(M) action in $\mathcal{N} = 2$ superspace reads

$$\begin{aligned}
S_{\text{CS}} + S_{\text{gf}} &= \frac{k}{4\pi} \left[\int d^3x d^4\theta \int_0^1 dt \operatorname{tr} V \left(\bar{D}^\alpha e^{-tV} D_\alpha e^{tV} + \frac{1}{2} \left(\frac{1}{\alpha} D^2 + \frac{1}{\hat{\alpha}} \bar{D}^2 \right) V \right) \right. \\
&\quad \left. - \int d^3x d^4\theta \int_0^1 dt \operatorname{tr} \hat{V} \left(\bar{D}^\alpha e^{-t\hat{V}} D_\alpha e^{t\hat{V}} + \frac{1}{2} \left(\frac{1}{\hat{\alpha}} D^2 + \frac{1}{\hat{\alpha}} \bar{D}^2 \right) \hat{V} \right) \right], \\
S_{\text{FP}} &= \frac{k}{4\pi} \left[\int d^3x d^4\theta \operatorname{tr} (c' + \bar{c}') L_{\frac{1}{2}V} (c + \bar{c} + \coth L_{\frac{1}{2}V} (c - \bar{c})) \right. \\
&\quad \left. - \int d^3x d^4\theta \operatorname{tr} (\hat{c}' + \hat{\bar{c}}') L_{\frac{1}{2}\hat{V}} (\hat{c} + \hat{\bar{c}} + \coth L_{\frac{1}{2}\hat{V}} (\hat{c} - \hat{\bar{c}})) \right] \\
S_{\text{mat}} &= \frac{k}{4\pi} \int d^3x d^4\theta \operatorname{tr} (\bar{Z}_A e^V Z^A e^{-\hat{V}} + \bar{W}^B e^{\hat{V}} W_B e^{-V}), \\
S_{\text{pot}} &= \frac{k}{4\pi} \frac{i}{2} \left[\int d^3x d^2\theta \epsilon_{AC} \epsilon^{BD} \operatorname{tr} Z^A W_B Z^C W_D \right. \\
&\quad \left. + \int d^3x d^2\bar{\theta} \epsilon^{AC} \epsilon_{BD} \operatorname{tr} \bar{Z}_A \bar{W}^B \bar{Z}_C \bar{W}^D \right], \tag{2.1}
\end{aligned}$$

where $L_V X = [V, X]$ and α and $\hat{\alpha}$ are gauge fixing parameters.

Many of the terms in this action have an infinite expansion, but for our purposes it is only necessary to retain the first few orders of any expansion. The first term in the Chern-Simons Lagrangian expands to

$$\int_0^1 dt \operatorname{tr} V \bar{D}^\alpha e^{-tV} D_\alpha e^{tV} = \frac{1}{2} \operatorname{tr} V \bar{D}^\alpha D_\alpha V - \frac{1}{6} \operatorname{tr} V \bar{D}^\alpha [V, D_\alpha V] + \dots \tag{2.2}$$

The quadratic piece in this expression, together with the α - and $\hat{\alpha}$ -dependent gauge fixing terms, determines the gauge superfield propagators. In order to simplify the D-algebra manipulations we will choose the Landau gauge where $\alpha = \hat{\alpha} = 0$. The leading expansion for the Fadeev-Popov action is

$$S_{\text{FP}} = \frac{k}{4\pi} \int d^3x d^4\theta \operatorname{tr} \left(\bar{c}' c - c' \bar{c} + \frac{1}{2} (c' + \bar{c}') [V, c + \bar{c}] \right) + \dots, \tag{2.3}$$

while the leading expansion for the matter action D -terms is

$$\begin{aligned}
S_{\text{mat}} &= \frac{k}{4\pi} \int d^3x d^4\theta \left[\operatorname{tr} \bar{Z}_A \left(Z^A + V Z^A - Z^A \hat{V} + \frac{1}{2} (V^2 Z^A + Z^A \hat{V}^2) - V Z^A \hat{V} \right) + \dots \right. \\
&\quad \left. + \operatorname{tr} \bar{W}^A \left(W_A + \hat{V} W_A - W_A V + \frac{1}{2} (\hat{V}^2 W_A + W_A V^2) - \hat{V} W_A V \right) \right. \\
&\quad \left. + \dots \right]. \tag{2.4}
\end{aligned}$$

We have collected the Feynman rules which follow from the action and the above expansions in appendix B. The supergraphs are then constructed from the Feynman rules and are reducible to ordinary integrals using standard D-algebra techniques [32].

The advantage of using superspace as opposed to the component approach is that the number of diagrams is significantly smaller. Furthermore, one can often find cancellation

patterns between different supergraphs or demonstrate finiteness theorems for classes of diagrams [16, 19]. Such generalized finiteness conditions [16] that follow from power counting arguments and some of their implications are summarized in section 4.1. They predict the finiteness of many diagrams and will be of great use to us in our calculations.

3 The dilatation operator and $h^2(\bar{\lambda}, \sigma)$

The dilatation operator \mathcal{D} is the natural tool to study the anomalous dimensions of composite operators in field theory. It can be defined as the operator that by acting on composite operators \mathcal{O}_a provides the matrix of scaling dimensions

$$\mathcal{D}\mathcal{O}_a = \Delta_a^b(\mathcal{O})\mathcal{O}_b . \quad (3.1)$$

Note that Δ_a^b leads in general to the mixing between operators. As known, the matrix of dimensions, and therefore the dilatation operator, can be extracted from the perturbative renormalization of the composite operators \mathcal{O}_a

$$\mathcal{O}_{a,\text{ren}} = \mathcal{Z}_a^b \mathcal{O}_{b,\text{bare}} , \quad \mathcal{Z} = \mathbf{1} + \bar{\lambda}^2 \mathcal{Z}_2 + \bar{\lambda}^4 \mathcal{Z}_4 + \dots . \quad (3.2)$$

The matrix \mathcal{Z} is such that $\mathcal{O}_{a,\text{ren}}$ is free from perturbative quantum divergences and can be computed in perturbation theory by means of standard methods. In this paper we use dimensional reduction with the space-time dimension D given by

$$D = 3 - 2\varepsilon , \quad (3.3)$$

in order to regularize quantum divergences that show up as inverse powers of ε in the limit $\varepsilon \rightarrow 0$. By introducing the 't Hooft mass μ and the dimensionful combination $\bar{\lambda}\mu^{2\varepsilon}$ the dilatation operator is then extracted from \mathcal{Z} as

$$\mathcal{D} = \mathcal{D}_{\text{classical}} + \mu \frac{d}{d\mu} \ln \mathcal{Z}(\bar{\lambda}\mu^{2\varepsilon}, \varepsilon) = \mathcal{D}_{\text{classical}} + \lim_{\varepsilon \rightarrow 0} \left[2\varepsilon \bar{\lambda} \frac{d}{d\bar{\lambda}} \ln \mathcal{Z}(\bar{\lambda}, \varepsilon) \right] . \quad (3.4)$$

In a loop expansion of the dilatation operator, the l th loop order is then simply given by the $\bar{\lambda}^{2l}$ coefficient of the $1/\varepsilon$ pole of $\ln \mathcal{Z}$ multiplied by $2l$. The higher order poles must be absent in $\ln \mathcal{Z}$; this will be later used as a consistency check for our result.

As discussed in the introduction, in the ABJ(M) models the dilatation operator can be mapped to the long range Hamiltonian of a spin-chain system for the whole $OSp(6|4)$ symmetry group [2, 10]. We focus on the $SU(2) \times SU(2)$ subsector where the magnons propagating along the spin chain form two sectors: the ones living on the odd sites belong to the first $SU(2)$, while those on the even sites are associated with the other $SU(2)$. As demonstrated in appendix F.1, in our four-loop analysis the two different types of magnons can be regarded as non-interacting, since the contributions to the dilatation operator of the respective diagrams that could lead to these interactions cancel. The all-loop Bethe Ansatz [5] predicts that such interactions start at eight loops. In analogy with the $\mathcal{N} = 4$ case, the spin-chain is interpreted as a quantum mechanical system in which the ground state of length $2L$ can be chosen to be

$$\Omega = \text{tr} (W_1 Z^1)^L . \quad (3.5)$$

With a single excitation W_2 of an odd site the momentum eigenstate is defined as

$$\psi_p = \sum_{k=0}^{L-1} e^{ipk} (W_1 Z^1)^k W_2 Z^1 (W_1 Z^1)^{L-k-1} \quad (3.6)$$

This describes a single magnon excitation with momentum p . The main difference between the $\mathcal{N} = 6$ CS and the $\mathcal{N} = 4$ SYM case is the existence in the former of two different $SU(2)$ excitations corresponding to the sectors mentioned above.

Up to four loops, the dilatation operator for a chain of length $2L$ then expands as

$$\mathcal{D} = L + \bar{\lambda}^2 (\mathcal{D}_{2,\text{odd}} + \mathcal{D}_{2,\text{even}}) + \bar{\lambda}^4 (\mathcal{D}_{4,\text{odd}}(\sigma) + \mathcal{D}_{4,\text{even}}(\sigma)) + \mathcal{O}(\bar{\lambda}^6) , \quad (3.7)$$

where the individual parts act non-trivially on odd and even sites only.

In the $\mathcal{N} = 4$ SYM case chiral functions have been introduced in [19] as a very convenient basis for the dilatation operator of the $SU(2)$ subsector. The chiral functions directly capture the structure of the chiral superfields in the Feynman diagrams. As in the $\mathcal{N} = 4$ SYM case, also in the $\mathcal{N} = 6$ CS case the elementary building block for the chiral function of the $SU(2) \times SU(2)$ subsector is constructed from the superpotential by contracting one chiral and one anti-chiral vertex with a single chiral propagator. The resulting flavour structure then yields the simplest non-trivial chiral function.

The chiral functions that are relevant to two loops in $\mathcal{N} = 4$ SYM and to four loops in $\mathcal{N} = 6$ CS theory turn out to have identical form in terms of the respective permutation structures and read

$$\begin{aligned} \chi(a, b) &= \{a, b\} - \{a\} - \{b\} + \{\} , \\ \chi(a) &= \{a\} - \{\} , \\ \chi() &= \{\} . \end{aligned} \quad (3.8)$$

However, the permutation structures in both theories slightly differ. In the $\mathcal{N} = 6$ CS case they are given by [15]

$$\{a_1, a_2, \dots, a_m\} = \sum_{i=0}^{L-1} P_{2i+a_1} P_{2i+a_1+2} P_{2i+a_2} P_{2i+a_2+2} \dots P_{2i+a_m} P_{2i+a_m+2} , \quad (3.9)$$

where we identify $L + i \equiv i$, such that the product of permutations, in which P_{aa+2} permutes the flavours at sites a and $a + 2$, is inserted at every second site of the cyclic spin chain of length $2L$.² The insertion at each second site thereby allows for the decomposition of the dilatation operator into two separate pieces acting only on odd or even sites as in (3.7). The decomposition of the dilatation operator to four loops [15] in terms of chiral functions then reads

$$\begin{aligned} \mathcal{D}_{2,\text{odd}} &= -\chi(1) , \\ \mathcal{D}_{2,\text{even}} &= -\chi(2) , \\ \mathcal{D}_{4,\text{odd}}(\sigma) &= -\chi(1, 3) - \chi(3, 1) + (2 - h_4(\sigma))\chi(1) , \\ \mathcal{D}_{4,\text{even}}(\sigma) &= -\chi(2, 4) - \chi(4, 2) + (2 - h_4(-\sigma))\chi(2) . \end{aligned} \quad (3.11)$$

²Note that the permutation structures obey

$$\begin{aligned} \{\dots, a, b, \dots\} &= \{\dots, b, a, \dots\} , & |a - b| \neq 2 , \\ \{a, \dots, b\} &= \{a + 2n, \dots, b + 2n\} . \end{aligned} \quad (3.10)$$

The coefficients are thereby fixed by the magnon dispersion relation (1.3) in terms of the four-loop contribution $h_4(\sigma)$ of the a priori undetermined function $h^2(\bar{\lambda}, \sigma)$ in (1.6). As explained in [15] to obtain the above result, one just has to compare the expansion of the magnon dispersion relation to the momentum dependence when the individual terms are applied to the single magnon momentum eigenstate (3.6).

The function $h_4(\sigma)$ can be computed in the weak coupling limit from a direct perturbative calculation. This has been done by using component fields techniques in [15]. Here we present its calculation by using $\mathcal{N} = 2$ supergraphs. As in the component calculation [15], also here it suffices to only consider the odd part of the dilatation operator, i.e. the contributions with chiral functions that have odd integers as arguments.³ The supergraphs computation of the full $\mathcal{D}_{4,\text{odd}}$, and in particular of $h_4(\sigma)$, is the main result of our paper.

4 Feynman diagram calculation

Before starting with the explicit evaluation of Feynman diagrams we will summarize the previously mentioned finiteness conditions which allow us to disregard entire classes of diagrams.

4.1 Finiteness conditions

Based on power counting and structural properties of the Feynman rules, in [16] finiteness conditions for Feynman diagrams of $\mathcal{N} = 4$ SYM theory in terms of $\mathcal{N} = 1$ superfields and for $\mathcal{N} = 6$ CS theory in terms of $\mathcal{N} = 2$ superfields were derived. They hold for each diagram that contributes to the renormalization of chiral operators in the respective $SU(2)$ or $SU(2) \times SU(2)$ subsectors. In Landau gauge, such a diagram with interaction range $R \geq 2$ has no overall UV divergence, if at least one of the following criteria is matched:⁴

1. All of its chiral vertices are part of any loop.
2. One of its spinor derivative D_α is brought outside the loops.
3. The number of its spinor derivatives \bar{D}_α brought outside loops becomes equal or bigger than twice the number of chiral vertices that are not part of any loop.

In the flavour $SU(2) \times SU(2)$ subsector, a chiral vertex that is not part of any loop always generates flavour permutations and therefore a non-trivial chiral structure of the diagram. Analogously to the $\mathcal{N} = 4$ SYM case, the above finiteness conditions hence imply the following rule:

- All diagrams with interaction range $R \geq 2$ and trivial chiral structure $\chi(\cdot)$ are finite.

³As we mentioned before, odd and even site magnons are decoupled here, there is therefore no contribution with chiral functions with both odd and even integer arguments. We explicitly demonstrate their absence at four loops in appendix F.1.

⁴ $R \geq 2$ means, the composite operator is 1PI connected with the rest of the diagram, not including the non-interacting fields of the operator.

Note that together with the $1/\varepsilon$ poles we will also keep the higher order poles that display the presence of subdivergences. Here, to four-loop order the only appearing higher order poles are double poles. In appendix F.2 their cancellation in $\ln \mathcal{Z}$ will be explicitly demonstrated as an important consistency check of our calculation.

We note that, for the convenience of the reader, all the integrals appearing in the following are collected in the appendix C.

4.3.1 Range five interactions

At four loops there is only one supergraph that involves the maximum number of five neighbouring fields in the interaction. It is given by

$$S_{r5} = \begin{array}{c} \text{Diagram: A supergraph with five external legs and a central interaction vertex. The legs are arranged in a circular pattern around the vertex, with two legs on the left and three on the right. The diagram is drawn with thick black lines for the interaction and thin lines for the external legs. The legs are connected to the central vertex by curved lines. The diagram is shown in a box with a thick black border at the bottom and left sides. \end{array} \rightarrow \frac{(4\pi)^4}{k^4} (MN)^2 I_4 \chi(1, 3) = \frac{(\lambda \hat{\lambda})^2}{16} \left(-\frac{1}{2\varepsilon^2} + \frac{2}{\varepsilon} \right) \chi(1, 3) . \quad (4.3)$$

By taking into account the reflected diagram, the maximum range contribution to the renormalization constant is⁵

$$\mathcal{Z}_{r5, \text{odd}} = -(1 + \mathcal{R}) S_{r5} = \frac{(\lambda \hat{\lambda})^2}{16} \left(\frac{1}{2\varepsilon^2} - \frac{2}{\varepsilon} \right) (\chi(1, 3) + \chi(3, 1)) . \quad (4.4)$$

4.3.2 Range four interactions

There are four diagrams which have range four interactions and contribute to the structure $\chi(1)$ in the dilatation operator. According to section 4.1, for an overall UV divergence to be present, at least one purely chiral vertex has to remain outside the loops, and a single gauge propagator can not end up on an external leg. Therefore, the only relevant contributions turn out to be

$$\begin{aligned} S_{r4} &= \begin{array}{c} \text{Diagram: A supergraph with four external legs and a central interaction vertex. The legs are arranged in a circular pattern around the vertex, with two legs on the left and two on the right. The diagram is drawn with thick black lines for the interaction and thin lines for the external legs. The legs are connected to the central vertex by curved lines. The diagram is shown in a box with a thick black border at the bottom and left sides. \end{array} \rightarrow -\frac{(4\pi)^4}{k^4} M^3 N I_{4\mathbf{b}\mathbf{b}\mathbf{b}\mathbf{b}} \chi(1) = \frac{\lambda^3 \hat{\lambda}}{16} \left(-\frac{\pi^2}{2\varepsilon} \right) \chi(1) , \\ V_{r41} &= \begin{array}{c} \text{Diagram: A supergraph with four external legs and a central interaction vertex. The legs are arranged in a circular pattern around the vertex, with two legs on the left and two on the right. The diagram is drawn with thick black lines for the interaction and thin lines for the external legs. The legs are connected to the central vertex by curved lines. A wavy line (gauge propagator) connects two of the legs. The diagram is shown in a box with a thick black border at the bottom and left sides. \end{array} \rightarrow \frac{(4\pi)^4}{2k^4} M^3 N I_4 \chi(1) = \frac{\lambda^3 \hat{\lambda}}{32} \left(-\frac{1}{2\varepsilon^2} + \frac{2}{\varepsilon} \right) \chi(1) , \\ V_{r42} &= \begin{array}{c} \text{Diagram: A supergraph with four external legs and a central interaction vertex. The legs are arranged in a circular pattern around the vertex, with two legs on the left and two on the right. The diagram is drawn with thick black lines for the interaction and thin lines for the external legs. The legs are connected to the central vertex by curved lines. A wavy line (gauge propagator) connects two of the legs. The diagram is shown in a box with a thick black border at the bottom and left sides. \end{array} \rightarrow \frac{(4\pi)^4}{2k^4} M^3 N I_4 \chi(1) = \frac{\lambda^3 \hat{\lambda}}{32} \left(-\frac{1}{2\varepsilon^2} + \frac{2}{\varepsilon} \right) \chi(1) , \\ V_{r43} &= \begin{array}{c} \text{Diagram: A supergraph with four external legs and a central interaction vertex. The legs are arranged in a circular pattern around the vertex, with two legs on the left and two on the right. The diagram is drawn with thick black lines for the interaction and thin lines for the external legs. The legs are connected to the central vertex by curved lines. A wavy line (gauge propagator) connects two of the legs. The diagram is shown in a box with a thick black border at the bottom and left sides. \end{array} \rightarrow \frac{(4\pi)^4}{k^4} M^3 N I_{42\mathbf{b}\mathbf{b}\mathbf{d}} \chi(1) = \frac{\lambda^3 \hat{\lambda}}{16} \left(\frac{1}{2\varepsilon^2} - \frac{1}{\varepsilon} \left(2 - \frac{\pi^2}{4} \right) \right) \chi(1) . \end{aligned} \quad (4.5)$$

⁵By \mathcal{R} we indicate the reflection of a supergraph at the vertical axis. As in [15], the operation preserves the type of chiral function, i.e. if it belongs to the odd or even sector. In case of an even number of neighbours interacting with each other the operation therefore involves a shift of the interaction by one site along the composite operator. Effectively, \mathcal{R} therefore exchanges λ with $\hat{\lambda}$ and $\chi(a, b)$ with $\chi(b, a)$.

Also in this case one has to consider the diagrams obtained by reflecting the previous ones. The total contribution to the renormalization constant is then

$$\mathcal{Z}_{r4,\text{odd}} = \frac{\lambda\hat{\lambda}}{16}(\lambda^2 + \hat{\lambda}^2)\frac{\pi^2}{4\epsilon}\chi(1). \quad (4.6)$$

4.3.3 Range three interactions

The range three interactions arise from two-loop corrections to the propagators and vertices involved in the two-loop diagram (4.1). It is important to note that, due to the finiteness rules of section 4.1, overall UV divergences can arise only from corrections to the lower vertex or one of the three lower chiral propagators. According to the analysis of [31], the two-loop corrections to the chiral two- and four-point functions are plagued by IR divergences even if free of UV poles. This is due to the particular structure of the gauge superfield propagator and cubic vertices in $\mathcal{N} = 2$ superspace. We stress that IR divergences do not appear in component fields [15], since in three dimensions IR dangerous cubic vertices contribute non-trivial momentum factors to the numerators of the loop integrals. In superspace, the appearance of IR divergences in intermediate steps can be cured by using a non-standard gauge fixing procedure first introduced in four dimensions in [40] and adapted in [31] to the three-dimensional case. Since we are interested only in the overall UV divergences of the diagrams, a computational strategy could be to ignore purely IR divergent diagrams and to IR-regulate diagrams that involve both UV and IR divergences in such a way as to extract the purely UV poles. For example, this is illustrated in appendix C.2 where we can regulate the IR divergences by inserting external momenta in IR divergent diagrams. However, in the main body of the paper we have decided to keep track of the IR divergences and check at the end their cancellation. Such a check is described in appendix E.

The interested reader should look at appendix D for a description of the two-loop corrections to the two- and four-point functions needed in the calculations of this section.

The contributions with only UV divergences are given by

$$\begin{aligned}
S_{r3} &= \begin{array}{c} \text{Diagram: A semi-circle with a loop on the left side and a thick horizontal line at the bottom.} \end{array} \rightarrow -\frac{2(4\pi)^4}{k^4} M^3 N I_{42\mathbf{b}\mathbf{b}\mathbf{b}\mathbf{2}} \chi(1) = \frac{\lambda^3 \hat{\lambda}}{16} \left(-\frac{\pi^2}{2\varepsilon} \right) \chi(1), \\
V_{r31a} &= \begin{array}{c} \text{Diagram: A semi-circle with a loop on the right side and a thick horizontal line at the bottom.} \end{array} \rightarrow \frac{(4\pi)^4}{2k^4} M^3 N I_4 \chi(1) = \frac{\lambda^3 \hat{\lambda}}{16} \left(-\frac{1}{4\varepsilon^2} + \frac{1}{\varepsilon} \right) \chi(1), \\
V_{r31b} &= \begin{array}{c} \text{Diagram: A semi-circle with a loop on the left side and a thick horizontal line at the bottom.} \end{array} \rightarrow \frac{(4\pi)^4}{k^4} M^3 N (I_4 + I_{42\mathbf{b}\mathbf{b}\mathbf{d}}) \chi(1) = \frac{\lambda^3 \hat{\lambda}}{16} \frac{\pi^2}{4\varepsilon} \chi(1), \\
V_{r32a} &= \begin{array}{c} \text{Diagram: A semi-circle with a loop on the right side and a thick horizontal line at the bottom.} \end{array} \rightarrow \frac{(4\pi)^4}{k^4} M^3 N I_{42\mathbf{b}\mathbf{b}\mathbf{d}} \chi(1) = \frac{\lambda^3 \hat{\lambda}}{16} \left(\frac{1}{2\varepsilon^2} + \frac{1}{\varepsilon} \left(-2 + \frac{\pi^2}{4} \right) \right) \chi(1), \\
V_{r32b} &= \begin{array}{c} \text{Diagram: A semi-circle with a loop on the left side and a thick horizontal line at the bottom.} \end{array} \rightarrow -\frac{(4\pi)^4}{2k^4} M^3 N I_{422\mathbf{q}\mathbf{t}\mathbf{r}\mathbf{A}\mathbf{B}\mathbf{C}\mathbf{D}} \chi(1) = \frac{\lambda^3 \hat{\lambda}}{16} \left(-\frac{\pi^2}{6\varepsilon} \right) \chi(1), \\
V_{r33a} &= \begin{array}{c} \text{Diagram: A semi-circle with a loop on the right side and a thick horizontal line at the bottom.} \end{array} \rightarrow \frac{(4\pi)^4}{k^4} (MN)^2 I_{422\mathbf{q}\mathbf{t}\mathbf{r}\mathbf{A}\mathbf{B}\mathbf{b}\mathbf{d}} \chi(1) \\
&= \frac{(\lambda \hat{\lambda})^2}{16} \left(-\frac{1}{\varepsilon^2} + \frac{1}{\varepsilon} \left(4 - \frac{2\pi^2}{3} \right) \right) \chi(1), \\
V_{r33b} &= \begin{array}{c} \text{Diagram: A semi-circle with a loop on the left side and a thick horizontal line at the bottom.} \end{array} \rightarrow \frac{(4\pi)^4}{k^4} (MN)^2 I_{422\mathbf{q}\mathbf{t}\mathbf{r}\mathbf{A}\mathbf{B}\mathbf{C}\mathbf{D}} \chi(1) = \frac{(\lambda \hat{\lambda})^2 \pi^2}{16 \cdot 3\varepsilon} \chi(1), \\
V_{r34} &= \begin{array}{c} \text{Diagram: A semi-circle with a loop on the right side and a thick horizontal line at the bottom.} \end{array} \rightarrow \frac{(4\pi)^4}{k^4} (MN)^2 \left(2I_{42\mathbf{b}\mathbf{b}\mathbf{e}} - I_{422\mathbf{q}\mathbf{t}\mathbf{r}\mathbf{A}\mathbf{B}\mathbf{b}\mathbf{d}} \right. \\
&\quad \left. + 2(2I_{221\mathbf{b}\mathbf{e}} - I_{221\mathbf{d}\mathbf{c}})G(2-2\lambda, 1)G(2-3\lambda, 1) \right. \\
&\quad \left. - 2(I_{42\mathbf{b}\mathbf{b}\mathbf{d}} + I_{42\mathbf{b}\mathbf{b}\mathbf{e}}) \right) \chi(1) \\
&= \frac{(\lambda \hat{\lambda})^2}{16} \left(-\frac{\pi^2}{3\varepsilon} \right) \chi(1).
\end{aligned} \tag{4.7}$$

The contributions with both UV and IR divergences are given by

$$\begin{aligned}
V_{r35} &= \begin{array}{c} \text{Diagram: A vertical line with a loop at the top and a horizontal line at the bottom. A small arrow points to the loop.} \end{array} \rightarrow -\frac{(4\pi)^4}{k^4} (MN(4MN - M^2)) (I_4 - I_{4\text{UVIR}} + I_{42\text{bbd}}) \chi(1) \\
&= \frac{\lambda\hat{\lambda}}{16} (4\lambda\hat{\lambda} - \lambda^2) \left(-\frac{1}{2\varepsilon^2} + \frac{2}{\varepsilon} \left(-2 - \frac{\pi^2}{8} + \gamma - \ln 4\pi \right) \right) \chi(1) , \\
V_{r36} &= \begin{array}{c} \text{Diagram: A vertical line with a loop at the top and a horizontal line at the bottom. A small black dot is on the horizontal line.} \end{array} \rightarrow \frac{(4\pi)^4}{k^4} MN \left(2MN I_{4\text{bbb}} - \frac{1}{2} (8MN - (M^2 + N^2)) I_{4\text{UVIR}} \right) \chi(1) \\
&= \frac{\lambda\hat{\lambda}}{16} \left(\lambda\hat{\lambda} \frac{\pi^2}{\varepsilon} + (8\lambda\hat{\lambda} - (\lambda^2 + \hat{\lambda}^2)) \left(\frac{1}{4\varepsilon^2} + \frac{1}{\varepsilon} (2 - \gamma + \ln 4\pi) \right) \right) \chi(1) .
\end{aligned} \tag{4.8}$$

Note that the expressions for the integrals that appear in the results have their UV subdivergences subtracted. The suffix UVIR appears on integrals which due to different arrangements of their external momenta contribute both UV and IR divergences. The UV poles can be extracted by adding external momentum to the cubic vertex which causes the IR divergence, i.e. one replaces $I_{4\text{UVIR}} \rightarrow I_4$. This then yields

$$\begin{aligned}
V_{r35}^{\text{UV}} &= \frac{\lambda\hat{\lambda}}{16} (4\lambda\hat{\lambda} - \lambda^2) \left(-\frac{1}{2\varepsilon^2} + \frac{1}{\varepsilon} \left(2 - \frac{\pi^2}{4} \right) \right) \chi(1) , \\
V_{r36}^{\text{UV}} &= \frac{\lambda\hat{\lambda}}{16} \left(\lambda\hat{\lambda} \frac{\pi^2}{\varepsilon} + (8\lambda\hat{\lambda} - (\lambda^2 + \hat{\lambda}^2)) \left(\frac{1}{4\varepsilon^2} - \frac{1}{\varepsilon} \right) \right) \chi(1) ,
\end{aligned} \tag{4.9}$$

In appendix E we explicitly demonstrate that this result is also obtained if instead of choosing an IR safe momentum configuration all relevant diagrams with IR divergence are considered, i.e. the IR divergences cancel out in the final result.

The contribution of the range three interactions to the renormalization constant \mathcal{Z} is then given by

$$\begin{aligned}
\mathcal{Z}_{r3,\text{odd}} &= -(1 + \mathcal{R}) (S_{r3} + V_{r31a} + V_{r31b} + V_{r32a} + 2V_{r32b} + 2V_{r34} + V_{r35}^{\text{UV}}) \\
&\quad - V_{r33a} - V_{r33b} - 3V_{r36}^{\text{UV}} \\
&= \frac{\lambda\hat{\lambda}}{16} \left(\lambda\hat{\lambda} \left(-\frac{1}{\varepsilon^2} + \frac{1}{\varepsilon} \left(4 + \frac{2\pi^2}{3} \right) \right) + (\lambda^2 + \hat{\lambda}^2) \frac{\pi^2}{12\varepsilon} \right) \chi(1) .
\end{aligned} \tag{4.10}$$

4.4 Final result

We are now ready to put together the parts of our calculations necessary to extract the four-loop dilatation operator. As discussed before the dilatation operator for odd sites is obtained by extracting the $1/\varepsilon$ pole from the renormalization constant. Summing up the contributions to the $1/\varepsilon$ pole from (4.4), (4.6) and (4.10), we obtain

$$\begin{aligned}
\bar{\lambda}^4 \mathcal{Z}_{4,\text{odd}}|_{\frac{1}{\varepsilon}} &= (\mathcal{Z}_{r5,\text{odd}} + \mathcal{Z}_{r4,\text{odd}} + \mathcal{Z}_{r3,\text{odd}})|_{\frac{1}{\varepsilon}} \\
&= \frac{\lambda\hat{\lambda}}{16\varepsilon} \left[-2\lambda\hat{\lambda} (\chi(1,3) + \chi(3,1)) + \left(\lambda\hat{\lambda} \left(4 + \frac{2\pi^2}{3} \right) + (\lambda^2 + \hat{\lambda}^2) \frac{\pi^2}{3} \right) \chi(1) \right] ,
\end{aligned} \tag{4.11}$$

that, rewritten in terms of $\bar{\lambda}$ and σ of (1.2), gives

$$\bar{\lambda}^4 \mathcal{Z}_{4,\text{odd}}|_{\frac{1}{\varepsilon}} = \frac{\bar{\lambda}^4}{16\varepsilon} \left[-2(\chi(1,3) + \chi(3,1)) + \left(4\left(1 + \frac{\pi^2}{3}\right) + \sigma^2 \frac{\pi^2}{3} \right) \chi(1) \right]. \quad (4.12)$$

As already observed, in the $\ln \mathcal{Z}$ the higher order poles must be absent. This is a useful consistency check of our computation. Additional diagrams that do not contribute to the dilatation operator but have non-vanishing double poles have to be taken into account. Some of them consist of two separate two-loop interactions. Furthermore, one has to consider the diagrams that lead to interactions between magnons at odd and even sites and contribute only to the double pole when summed up. In appendix F, we prove that when all these double poles are taken into account, their sum is indeed cancelled by the two-loop contribution in the expansion of $\ln \mathcal{Z}$. The dilatation operator for odd sites is then obtained from (4.12) by multiplying the $1/\varepsilon$ pole by 8. With $\zeta(2) = \frac{\pi^2}{6}$, it reads

$$\mathcal{D}_{4,\text{odd}}(\sigma) = (2 + (4 + \sigma^2)\zeta(2))\chi(1) - \chi(1,3) - \chi(3,1). \quad (4.13)$$

By comparing the previous result with equation (3.11) we read off the four-loop coefficient of the function $h^2(\bar{\lambda}, \sigma)$

$$h_4(\sigma) = -(4 + \sigma^2)\zeta(2). \quad (4.14)$$

This result coincides with the one computed in [15]. It is interesting to note that, in contrast to the component calculation in [15], the integrals that contribute here to the dilatation operator show a correlation between the quadratic and the rational simple pole in ε : their relative coefficient is always -4 as for the simplest four-loop integral I_4 in (C.4). The rational term in (4.13) and therefore its absence in (4.14) is hence correlated with the quadratic pole that itself is determined by the two-loop result (F.5).

5 Possible scenarios for an all-loop function

In this section we discuss our attempts to find an all-loop function for $h^2(\bar{\lambda}, \sigma)$.

In the ABJM case where $\sigma = 0$, $h^2(\bar{\lambda}, 0) = h^2(\lambda)$, there is a surprisingly simple function that matches the weak coupling behavior up to four-loop order and also matches the leading strong coupling behavior. To this end we define $t \equiv 2\pi i\lambda$, which is a natural variable that also appears in expressions for supersymmetric ABJ(M) Wilson loops [26, 28, 29]. We then consider a rescaled function $g(t) = (2\pi)^2 h^2(\lambda)$. In terms of $g(t)$ the magnon dispersion relation becomes

$$\varepsilon(p) = \sqrt{\frac{1}{4} + \frac{g(t)}{\pi^2} \sin^2 \frac{p}{2}}, \quad (5.1)$$

and so has a form more in line with the $\mathcal{N} = 4$ dispersion relation where in that case $g(t)$ in (5.1) is replaced with λ .

In terms of $g(t)$, the proposed all-loop function is

$$g(t) = -(1-t) \log(1-t) - (1+t) \log(1+t), \quad (5.2)$$

whose weak coupling expansion is

$$\begin{aligned}
g(t) &= -\sum_{n=1}^{\infty} \frac{t^{2n}}{n(2n-1)} = -t^2 - \frac{1}{6}t^4 - \frac{1}{15}t^6 + \mathcal{O}(t^8) \\
&= (2\pi)^2 (\lambda^2 - 4\zeta(2)\lambda^4 + 6\zeta(4)\lambda^6 + \mathcal{O}(\bar{\lambda}^8)) .
\end{aligned}
\tag{5.3}$$

An obvious test is to compute $h^2(\lambda)$ to six-loop order, where the all-loop function in (5.2) predicts the value $h_6 = \frac{(2\pi)^4}{15}$. A six-loop computation is admittedly very difficult, but we believe it is manageable using the $\mathcal{N} = 2$ superspace formulation.

At strong coupling the expansion is

$$\begin{aligned}
g(t) &= -i\pi t - 2 \log t - 2 + \mathcal{O}(t^{-1}) \\
&= (2\pi)^2 \left(\frac{\lambda}{2} - \frac{1}{(2\pi)^2} \log(2\pi\lambda) - 2 + \mathcal{O}(\lambda^{-1}) \right) .
\end{aligned}
\tag{5.4}$$

The dominant term agrees with the leading strong coupling expansion from the string sigma-model. But also observe that the first correction corresponds to a two-loop contribution; a one-loop correction is absent. This disagrees with the prediction in [24] arising from the one-loop correction to the energy for a folded-string [25, 41–44]. In this language one would expect a $g(t)$ with leading asymptotic expansion

$$g(t) = -i\pi t - 2\sqrt{-i\pi t} \ln(2) + \dots .
\tag{5.5}$$

However, if one chooses a different prescription for summing over mode frequencies, where one essentially groups the modes into heavy and light [25], then $g(t)$ no longer has the \sqrt{t} term, agreeing with the large t expansion (5.4).⁶

The function in (5.2) does not appear to have an easy generalization to the ABJ case where $\sigma \neq 0$. Such a function would be expected to be invariant under the transformation [8]

$$\lambda \rightarrow \hat{\lambda} , \quad \hat{\lambda} \rightarrow 2\hat{\lambda} - \lambda + 1 .
\tag{5.6}$$

Under (5.6) the perturbative regime is mapped into strong coupling, making its verification difficult. Some evidence that $h^2(\bar{\lambda}, \sigma)$ is consistent with (5.6) was presented in [48]. One possible hint about the all-loop structure is that the four-loop contribution to $h^2(\bar{\lambda}, \sigma)$ can be rewritten as

$$\bar{\lambda}^4(4 + \sigma^2) = \lambda\hat{\lambda}(\lambda + \hat{\lambda})^2 .
\tag{5.7}$$

which is zero if $\lambda = -\hat{\lambda}$. It would be interesting to see if the higher order corrections remain zero under this condition. However, it is not clear how this could square with the strong coupling behavior nor with an invariance under the transformation in (5.6).

Another possibility is that $h^2(\bar{\lambda}, \sigma)$ is somehow related to recent results concerning supersymmetric Wilson loops in the ABJ(M) models. In this latter case, it was found using localization [49, 50] that the Wilson loop expectation value could be reduced to

⁶See [45] for a further discussion of this. These authors also show that the same choices of prescriptions appear in finite size corrections for giant magnons [46, 47] and lead to the same one-loop contributions to $h^2(\lambda)$.

a matrix model on a Lens space [26]. This matrix model is solvable in the planar limit [51, 52] and hence all-loop predictions can be extracted. In particular, for ABJM the perturbative free energy of the matrix model is [28]

$$F(t) = N^2 \left(\log(t) + \frac{1}{36}t^2 + \mathcal{O}(t^4) \right). \quad (5.8)$$

It is tempting to look for a connection between $F(t)$ and $g(t)$. One might try

$$(g(t))^{1/2} = -\frac{i}{N^2}t^2 \frac{\partial F}{\partial t} = -it - \frac{i}{18}t^3 + \mathcal{O}(t^5). \quad (5.9)$$

The full expansion also is maximally transcendental, but here one finds that the t^3 term is off by a factor of $2/3$. At strong coupling the free energy is asymptotically [29]

$$F(t) \approx -N^2 \frac{2\pi^{3/2}}{3} (-it)^{-1/2}. \quad (5.10)$$

Applying the same rule as in (5.9) one finds

$$(g(t))^{1/2} = -\frac{i}{N^2}t^2 \frac{\partial F}{\partial t} \approx \frac{\pi}{3}(-i\pi t)^{1/2}, \quad (5.11)$$

which differs by an overall factor of $\pi/3$ from the square root of the leading term in (5.4).

6 Wrapping interactions

To obtain the complete four-loop spectrum of operators in the $SU(2) \times SU(2)$ subsector, we have to consider the wrapping interactions for the non-protected operators that consist of up to four elementary fields. The only non-trivial operator is in the **20** of $SU(4)$ and has $L = 2$, i.e. exactly four elementary fields.

The only wrapping diagrams which according to the initially discussed finiteness theorems based on power counting can contribute to the dilatation operator are given

by

$$\begin{aligned}
W_1 &= \text{Diagram 1} \rightarrow -\frac{2(4\pi)^4}{k^4}(MN)^2 I_4 \chi(1) = \frac{(\lambda\hat{\lambda})^4}{16} \left(\frac{1}{\varepsilon^2} - \frac{4}{\varepsilon} \right) \chi(1) , \\
W_2 &= \text{Diagram 2} \rightarrow -\frac{2(4\pi)^4}{k^4}(MN)^2 I_{42\mathbf{b}\mathbf{b}\mathbf{0}cd} \chi(1) = \frac{(\lambda\hat{\lambda})^4}{16} \left(-\frac{1}{2\varepsilon^2} + \frac{3}{\varepsilon} \right) \chi(1) , \\
W_3 &= \text{Diagram 3} \rightarrow \frac{(4\pi)^4}{k^4}(MN)^2 I_{422\mathbf{b}\mathbf{tr}ABcd} \chi(1) = \frac{(\lambda\hat{\lambda})^4}{16} \left(\frac{1}{\varepsilon^2} - \frac{2}{\varepsilon} \right) \chi(1) , \\
W_4 &= \text{Diagram 4} \rightarrow -\frac{2(4\pi)^4}{k^4}(MN)^2 I_4 \chi(1) = \frac{(\lambda\hat{\lambda})^4}{16} \left(\frac{1}{\varepsilon^2} - \frac{4}{\varepsilon} \right) \chi(1) , \\
W_5 &= \text{Diagram 5} \rightarrow \frac{(4\pi)^4}{k^4}(MN)^2 I_{422\mathbf{q}\mathbf{tr}ABbd} \chi(1) = \frac{(\lambda\hat{\lambda})^4}{16} \left(-\frac{1}{\varepsilon^2} + \frac{1}{\varepsilon} \left(4 - \frac{2}{3}\pi^2 \right) \right) \chi(1) .
\end{aligned} \tag{6.1}$$

There are four distinct diagrams of type W_2 and two of type W_3 . The sum of the wrapping diagrams is therefore given by

$$W = W_1 + 4W_2 + 2W_3 + W_4 + W_5 = \frac{(\lambda\hat{\lambda})^4}{16} \left[\frac{1}{\varepsilon^2} + \frac{2}{\varepsilon} \left(2 - \frac{\pi^2}{3} \right) \right] \chi(1) . \tag{6.2}$$

Multiplying the $1/\varepsilon$ pole of W by -8 , we obtain the wrapping contribution to the dilatation operator. It reads

$$\mathcal{D}_{4,\text{odd}}^{\mathbf{w}} = -(2 - 2\zeta(2))\chi(1) . \tag{6.3}$$

Now, by subtracting from (4.13) the range five contribution and inserting $h_4(\sigma) = -(4 + \sigma^2)\zeta(2)$, the subtracted dilatation operator becomes

$$\mathcal{D}_{4,\text{odd}}^{\text{sub}}(\sigma) = (2 - h_4(\sigma))\chi(1) = (2 + (4 + \sigma^2)\zeta(2))\chi(1) . \tag{6.4}$$

The dilatation operator for length four states then reads

$$\mathcal{D}_{4,\text{odd}}^{\text{range } 4}(\sigma) = \mathcal{D}_{4,\text{odd}}^{\text{sub}}(\sigma) + \mathcal{D}_{4,\text{odd}}^{\mathbf{w}} = (6 + \sigma^2)\zeta(2)\chi(1) , \tag{6.5}$$

and it coincides with the results obtained in terms of component fields [14, 15].

Note that the separation of the dilatation operator into wrapping and subtracted parts differs in the superfield calculation from the one obtained in component fields in [14, 15]. The sum of the two terms is, however, the same in the two calculations, and hence the resulting anomalous dimensions for operators with length $2L = 4$ agree.

7 Conclusions

In this paper we have computed $h_4(\sigma)$ using the $\mathcal{N} = 2$ superspace formalism. The computation is greatly simplified from the component version [14, 15] because the manifest supersymmetry in combination with finiteness conditions leads to a large reduction in the number of Feynman diagrams.

With this reduction in diagrams, it should be possible to tackle more challenging computations, including the six-loop term $h_6(\sigma)$. Six loops would give one more data point and might provide further insights into an all-loop function.

Alternatively, one could also apply the superspace formalism to four loops but beyond the $SU(2) \times SU(2)$ sector. This would not give us further information on $h^2(\bar{\lambda}, \sigma)$, but it would provide a check of higher-loop integrability in both ABJM and ABJ models. One reason that integrability in the ABJ case is not assured is because at strong coupling a nonzero σ would correspond to a nonzero θ -angle for the world-sheet, which is normally thought to destroy integrability. However, at the lowest order in perturbation theory, the spin-chain is integrable in all sectors, even when $\sigma \neq 0$ [10, 11]. It would be interesting to see how this plays out at higher loops.

Acknowledgements

The work of M. L., A. M. and A. S. has been supported in part by the Italian MIUR-PRIN contract 20075ATT78. The research of J. A. M. is supported in part by the Swedish research council and the STINT foundation. J. A. M. thanks the CTP at MIT and Nordita during the workshop “Integrability in String and Gauge Theories; AdS/CFT Duality and its applications” for kind hospitality during the course of this work. O. O. S. thanks the Centre for Mathematical Science at City University in London for kind hospitality during course of this work. C. S. thanks the department of Physics in Milan for kind hospitality during the course of this work. During the first stages of this work, G. T.-M. was supported by the J. S. Toll Professorship, the University of Maryland Center for String & Particle Theory, and National Science Foundation Grant PHY-0354401. After March 2010, G. T.-M. was supported by the European Commission Marie Curie Intra-European Fellowships under the contract PIEF-GA-2009-236454. G. T.-M. thanks the department of Physics in Milan for support and hospitality at different stages of this work.

A Conventions and identities

We use three-dimensional spinor and superspace notations adapted from [32]. We directly work in the Wick rotated Euclidean space-time with metric $g_{\mu\nu} = g^{\mu\nu} = \text{diag}(1, 1, 1)$. For a given three-dimensional spinor field ψ_α , we raise and lower spinor indices as

$$\psi^\alpha = C^{\alpha\beta} \psi_\beta, \quad \psi_\alpha = \psi^\beta C_{\beta\alpha}. \quad (\text{A.1})$$

where we use the spinor metric $C^{\alpha\beta}$ defined by

$$C^{\alpha\beta} = \begin{pmatrix} 0 & i \\ -i & 0 \end{pmatrix}, \quad C_{\alpha\beta} = \begin{pmatrix} 0 & -i \\ i & 0 \end{pmatrix}, \quad (\text{A.2})$$

For the contraction of spinor indices we use the notation

$$\psi\chi = \psi^\alpha\chi_\alpha = \chi^\alpha\psi_\alpha = \chi\psi, \quad \psi^2 = \frac{1}{2}\psi^\alpha\psi_\alpha. \quad (\text{A.3})$$

The γ -matrices obey the relation

$$(\gamma^\mu)^\alpha{}_\gamma(\gamma^\nu)^\gamma{}_\beta = -g^{\mu\nu}\delta^\alpha{}_\beta - \epsilon^{\mu\nu\rho}(\gamma_\rho)^\alpha{}_\beta. \quad (\text{A.4})$$

where the Levi-Civita tensor is such that $\epsilon^{012} = 1$. When one spinor index is lowered or raised the γ -matrices are symmetric

$$(\gamma^\mu)_{\alpha\beta} = (\gamma^\mu)_\alpha{}^\delta C_{\delta\beta} = (\gamma^\mu)_{\beta\alpha}, \quad (\gamma^\mu)^{\alpha\beta} = C^{\alpha\delta}(\gamma^\mu)_{\delta}{}^\beta = (\gamma^\mu)^{\beta\alpha}. \quad (\text{A.5})$$

The trace of product of γ -matrices satisfies

$$\begin{aligned} \text{tr}(\gamma^\mu\gamma^\nu) &= (\gamma^\mu)^\alpha{}_\beta(\gamma^\nu)^\beta{}_\alpha = -2g^{\mu\nu}, \\ \text{tr}(\gamma^\mu\gamma^\nu\gamma^\rho) &= -(\gamma^\mu)^\alpha{}_\beta(\gamma^\nu)^\beta{}_\gamma(\gamma^\rho)^\gamma{}_\alpha = -2\epsilon^{\mu\nu\rho}, \\ \text{tr}(\gamma^\mu\gamma^\nu\gamma^\rho\gamma^\sigma) &= (\gamma^\mu)^\alpha{}_\beta(\gamma^\nu)^\beta{}_\gamma(\gamma^\rho)^\gamma{}_\delta(\gamma^\sigma)^\delta{}_\alpha = 2(g^{\mu\nu}g^{\rho\sigma} - g^{\mu\rho}g^{\nu\sigma} + g^{\mu\sigma}g^{\nu\rho}). \end{aligned} \quad (\text{A.6})$$

We use the convention that the first of two contracted indices is always an upper index; this is used in the previous formulas in the definition of the trace of products of gamma matrices and it is very useful for D-algebra manipulations [32].

Using the γ -matrices we can move from vector to bi-spinor indices thanks to the following definitions

$$\begin{aligned} x^{\alpha\beta} &= \frac{1}{2}(\gamma_\mu)^{\alpha\beta}x^\mu, & x^\mu &= (\gamma^\mu)_{\alpha\beta}x^{\alpha\beta}, \\ p_{\alpha\beta} &= (\gamma^\mu)_{\alpha\beta}p_\mu, & p_\mu &= \frac{1}{2}(\gamma_\mu)^{\alpha\beta}p_{\alpha\beta}, \\ A_{\alpha\beta} &= \frac{1}{\sqrt{2}}(\gamma^\mu)_{\alpha\beta}A_\mu, & A_\mu &= \frac{1}{\sqrt{2}}(\gamma_\mu)^{\alpha\beta}A_{\alpha\beta}, \end{aligned} \quad (\text{A.7})$$

respectively for coordinates, momenta and fields. As usual, here the momentum p_μ is related to the vector derivative $\partial_\mu = \frac{\partial}{\partial x^\mu}$ by Fourier transform and $p_\mu = i\partial_\mu$.

The three-dimensional, $\mathcal{N} = 2$ superspace spinor covariant derivatives D_α, \bar{D}_α satisfy the algebra

$$\{D_\alpha, D_\beta\} = \{\bar{D}_\alpha, \bar{D}_\beta\} = 0, \quad \{D_\alpha, \bar{D}_\beta\} = p_{\alpha\beta}. \quad (\text{A.8})$$

The metric ϵ_{AB} for the SU(2) flavour indices is given by

$$\epsilon_{12} = 1, \quad \epsilon^{12} = 1, \quad \epsilon^{AB}\epsilon_{CD} = \delta_C^A\delta_D^B - \delta_D^A\delta_C^B. \quad (\text{A.9})$$

The flavour indices are raised and lowered as

$$\psi^A = \epsilon^{AB}\psi_B, \quad \psi_A = \psi^B\epsilon_{BA}. \quad (\text{A.10})$$

For the integration over the superspace our conventions are $\int d^2\theta = \frac{1}{2}\partial^\alpha\partial_\alpha$, $\int d^2\bar{\theta} = \frac{1}{2}\bar{\partial}^\alpha\bar{\partial}_\alpha$ and $\int d^4\theta = \int d^2\theta d^2\bar{\theta}$, such that

$$\begin{aligned}\int d^3x d^2\theta &= \int d^3x D^2|_{\theta=\bar{\theta}=0}, & \int d^3x d^2\bar{\theta} &= \int d^3x \bar{D}^2|_{\theta=\bar{\theta}=0}, \\ \int d^3x d^4\theta &= \int d^3x D^2\bar{D}^2|_{\theta=\bar{\theta}=0}.\end{aligned}\tag{A.11}$$

The θ -space δ -function is given by

$$\delta^4(\theta - \theta') = (\theta - \theta')^2(\bar{\theta} - \bar{\theta}')^2.\tag{A.12}$$

B Feynman rules in superspace

We use the Wick rotated Feynman rules, i.e. we have $e^{-iS} \rightarrow e^S$ in the path integral. The propagators are given by

$$\begin{aligned}\text{---}\overbrace{\text{---}}^{\text{---}}\text{---} &= \langle V(p)V(-p) \rangle = -\langle \hat{V}(p)\hat{V}(-p) \rangle = \frac{1}{p^2} D\bar{D}\delta^4(\theta_1 - \theta_2), \\ A\overrightarrow{\text{---}}_p^B &= \langle Z^B(p)\bar{Z}_A(-p) \rangle = \langle \bar{W}^B(p)W_A(-p) \rangle = \frac{\delta_A^B}{p^2}\delta^4(\theta_1 - \theta_2), \\ \text{---}\overleftarrow{\text{---}}_p &= \langle \bar{c}'(p)c(-p) \rangle = -\langle c'(p)\bar{c}(-p) \rangle \\ &= -\langle \hat{c}'(p)\hat{c}(-p) \rangle = \langle \hat{c}'(p)\hat{c}(-p) \rangle = \frac{1}{p^2}\delta^4(\theta_1 - \theta_2),\end{aligned}\tag{B.1}$$

where diagonality in the gauge group indices and a factor $\frac{4\pi}{k}$ for each propagator have been suppressed.

The vertices are obtained by taking the functional derivatives of the Wick rotated action (no factors of i) w.r.t. the corresponding superfields; we will give only the vertices involved in the computations of our paper. When a functional derivatives w.r.t. the (anti)-chiral superfields is taken, factors of $(D^2)\bar{D}^2$ are generated in the vertices.

Omitting factors $\frac{k}{4\pi}$, for the three point vertices we obtain

$$\begin{aligned}
V_{V^3} &= \left(\text{---} \begin{array}{c} \text{---} \text{---} \\ \text{---} \end{array} \text{---} - \text{---} \begin{array}{c} \text{---} \text{---} \\ \text{---} \end{array} \text{---} \right) \frac{1}{2} \text{tr} (T^a [T^b, T^c]) , \\
V_{VZ^B\bar{Z}_C} &= \text{---} \begin{array}{c} \text{---} \text{---} \\ \text{---} \end{array} \delta_B^C \text{tr} (T^a B^{\underline{b}} B_{\underline{c}}) , & V_{\hat{V}W_B\bar{W}^C} &= \text{---} \begin{array}{c} \text{---} \text{---} \\ \text{---} \end{array} \delta_C^B \text{tr} (T^{\hat{a}} B_{\underline{b}} B^{\underline{c}}) , \\
V_{\hat{V}\bar{Z}_B Z^C} &= \text{---} \begin{array}{c} \text{---} \text{---} \\ \text{---} \end{array} (-1) \delta_C^B \text{tr} (T^{\hat{a}} B_{\underline{b}} B^{\underline{c}}) , & V_{V\bar{W}^B W_C} &= \text{---} \begin{array}{c} \text{---} \text{---} \\ \text{---} \end{array} (-1) \delta_B^C \text{tr} (T^a B^{\underline{b}} B_{\underline{c}}) , \\
V_{V_{cc'}} &= \text{---} \begin{array}{c} \text{---} \text{---} \\ \text{---} \end{array} \frac{1}{2} \text{tr} (T^a [T^b, T^c]) , & V_{V_{c\bar{c}'}} &= \text{---} \begin{array}{c} \text{---} \text{---} \\ \text{---} \end{array} \frac{1}{2} \text{tr} (T^a [T^b, T^c]) , \\
V_{V_{\bar{c}c'}} &= \text{---} \begin{array}{c} \text{---} \text{---} \\ \text{---} \end{array} \frac{1}{2} \text{tr} (T^a [T^b, T^c]) , & V_{V_{\bar{c}\bar{c}'}} &= \text{---} \begin{array}{c} \text{---} \text{---} \\ \text{---} \end{array} \frac{1}{2} \text{tr} (T^a [T^b, T^c]) ,
\end{aligned} \tag{B.2}$$

where the colour indices are labeled (a, b, c) counter clockwise starting with the leg to the left. Besides the matrices T^a and $T^{\hat{a}}$ transforming in the adjoint of the respective gauge groups $U(M)$ and $U(N)$, we have introduced matrices $B^{\underline{a}}$ and $B_{\underline{a}}$, with underlined $\underline{a} = 1, \dots, MN$ indices that transform in the $(\mathbf{M}, \bar{\mathbf{N}})$ and $(\mathbf{N}, \bar{\mathbf{M}})$ of the gauge group $U(M) \times U(N)$. The previous notations are useful because one can effectively consider all the matrices to be the same for $M = N$ and then only at the end one can easily recover the different factors of M and N coming from the colour contractions.

The quartic vertices used in the paper are

$$\begin{aligned}
V_{V^2 Z^C \bar{Z}_D} &= \text{---} \begin{array}{c} \text{---} \text{---} \\ \text{---} \end{array} \frac{1}{2} \delta_C^D [\text{tr} (\{T^a, T^b\} B^{\underline{c}} B_{\underline{d}})] , \\
V_{\hat{V}^2 \bar{Z}_C Z^D} &= \text{---} \begin{array}{c} \text{---} \text{---} \\ \text{---} \end{array} \frac{1}{2} \delta_D^C [\text{tr} (\{T^{\hat{a}}, T^{\hat{b}}\} B_{\underline{c}} B^{\underline{d}})] , \\
V_{VZ^B \hat{V}\bar{Z}_D} &= \text{---} \begin{array}{c} \text{---} \text{---} \\ \text{---} \end{array} (-1) \delta_B^D \text{tr} (T^a B^{\underline{b}} T^{\hat{c}} B_{\underline{d}}) ,
\end{aligned} \tag{B.3}$$

where the colour indices are labeled (a, b, c, d) counter clockwise starting with the leg in the upper left corner. The vertices $V_{\hat{V}^2 W_C \bar{W}^D}$, $V_{V^2 \bar{W}^C W_D}$, $V_{\hat{V} W_B V \bar{W}^D}$ involving the W_A and \bar{W}^A superfields are respectively identical to the previous three vertices up to trivial modifications in the flavour and colour structures.

The quartic superpotential vertices are

$$\begin{aligned}
V_{Z^A W_B Z^C W_D} &= \begin{array}{c} \text{\scriptsize } D^2 \\ \diagup \quad \diagdown \\ \text{\scriptsize } \bar{D}^2 \quad \text{\scriptsize } D^2 \end{array} i\epsilon^{AC}\epsilon_{BD} [\text{tr}(B^{\underline{a}}B_{\underline{b}}B^{\underline{c}}B_{\underline{d}}) - \text{tr}(B^{\underline{c}}B_{\underline{b}}B^{\underline{a}}B_{\underline{d}})] , \\
V_{\bar{Z}_A \bar{W}^B \bar{Z}_C \bar{W}^D} &= \begin{array}{c} \text{\scriptsize } D^2 \\ \diagup \quad \diagdown \\ \text{\scriptsize } \bar{D}^2 \quad \text{\scriptsize } D^2 \end{array} i\epsilon_{AC}\epsilon^{BD} [\text{tr}(B_{\underline{a}}B^{\underline{b}}B_{\underline{c}}B^{\underline{d}}) - \text{tr}(B_{\underline{c}}B^{\underline{b}}B_{\underline{a}}B^{\underline{d}})] ,
\end{aligned} \tag{B.4}$$

where again the colour indices are labeled (a, b, c, d) counter clockwise starting with the leg in the upper left corner. Note also that, in a standard way, one of the $(D^2) \bar{D}^2$ factors has been absorbed into the (anti)chiral integration such that the integration measure of the (anti)chiral vertex is promoted to the full superspace measure.

C Integrals

In this section we collect the integrals required for our paper. The results are based on the Appendices H, I, J of [15] where the reader should look to have a complete description of the notations and results that we are using.

The integrals are computed by using dimensional regularization in Euclidean space with D dimensions and

$$D = 2(\lambda + 1) = 3 - 2\varepsilon , \quad \lambda = \frac{1}{2} - \varepsilon . \tag{C.1}$$

As usual we will expand the integrals in the limit $\varepsilon \rightarrow 0$ up to the order needed for our computations. The parameter λ in this appendix should not be confused with the 't Hooft coupling that appears in the main body of the paper. The integrals have a simple dependence on the external momentum p_μ which we will omit. Relations between four-loop expressions are understood to hold for the pole parts up to disregarded finite contributions.

C.1 Integrals with only UV divergences

We need the following two-loop integral

$$I_2 = \text{\scriptsize } \text{\textcircled{---}} = G(1, 1)G(1 - \lambda, 1) . \tag{C.2}$$

The reader can look at the appendix H of [15] for our notations in using the G -functions. Furthermore, we need the following two-loop integrals with two contracted momenta in

their numerators

$$\begin{aligned}
I_{221be} &= \text{Diagram} = \frac{1}{2}(-G_1(1, 1)G(1, 1) - G(1, 1)G_1(2 - \lambda, 1) + G_1(1, 1)G_1(2 - \lambda, 1)) , \\
I_{221dc} &= \text{Diagram} = -G_1(1, 1)G_1(2 - \lambda, 1) .
\end{aligned} \tag{C.3}$$

At four loops there are many integrals involved in the computations. Here we list the results for the pole parts of the UV logarithmically divergent integrals where the subdivergences have already been subtracted. Four-loop integrals with no momenta in their numerators are

$$\begin{aligned}
I_4 &= \text{Diagram} = \frac{1}{(8\pi)^4} \left(-\frac{1}{2\varepsilon^2} + \frac{2}{\varepsilon} \right) , \\
I_{4bbb} &= \text{Diagram} = \frac{1}{(8\pi)^4} \frac{\pi^2}{2\varepsilon} .
\end{aligned} \tag{C.4}$$

Four-loop integrals with two contracted momenta in their numerators are

$$\begin{aligned}
I_{42bbb2} &= \text{Diagram} = \frac{1}{(8\pi)^4} \frac{\pi^2}{4\varepsilon} , \\
I_{42bb0cd} &= \text{Diagram} = \frac{1}{(8\pi)^4} \left(\frac{1}{4\varepsilon^2} - \frac{3}{2\varepsilon} \right) , \\
I_{42bbd} &= \text{Diagram} = \frac{1}{(8\pi)^4} \left(\frac{1}{2\varepsilon^2} - \frac{1}{\varepsilon} \left(2 - \frac{\pi^2}{4} \right) \right) , \\
I_{42bbe} &= \text{Diagram} = \frac{1}{(8\pi)^4} \left(-\frac{1}{4\varepsilon^2} \right) .
\end{aligned} \tag{C.5}$$

Let us consider now four-loop integrals with four pairwise contracted momenta in their numerators. The following ones

$$I_{422bABcd} = \text{Diagram} , \quad I_{422bAcBd} = \text{Diagram} , \quad I_{422bAdBc} = \text{Diagram} , \tag{C.6}$$

appear in a fixed combination which can be recast into the form

$$\begin{aligned}
I_{422\mathbf{b}trABcd} &= -\text{tr} \left(\text{diagram} \right) = -2(I_{422\mathbf{b}ABcd} - I_{422\mathbf{b}AcBd} + I_{422\mathbf{b}AdBc}) \\
&= 2 \left(\text{diagram}_1 \right) + 2 \left(\text{diagram}_2 \right) - 4 \left(\text{diagram}_3 \right) = \frac{1}{(8\pi)^4} \left(\frac{1}{\varepsilon^2} - \frac{2}{\varepsilon} \right),
\end{aligned} \tag{C.7}$$

Here we have taken the trace of γ -matrices contracted with the momenta in the integral. We thereby read off the momenta in a cycle, but keep their direction as indicated by the arrows.

We also need the integrals

$$\begin{aligned}
I_{422\mathbf{q}ABbd} &= \left(\text{diagram}_1 \right) = \frac{1}{(8\pi)^4} \left(\frac{1}{4\varepsilon^2} + \frac{1}{4\varepsilon} \right), \\
I_{422\mathbf{q}AdBb} &= \left(\text{diagram}_2 \right) = \frac{1}{(8\pi)^4} \left(\frac{1}{2\varepsilon^2} - \frac{1}{\varepsilon} \left(1 - \frac{\pi^2}{4} \right) \right), \\
I_{422\mathbf{q}AbBd} &= \left(\text{diagram}_3 \right) = \frac{1}{(8\pi)^4} \left(\frac{1}{4\varepsilon^2} + \frac{1}{\varepsilon} \left(\frac{5}{4} - \frac{\pi^2}{12} \right) \right).
\end{aligned} \tag{C.8}$$

The linear combinations of integrals originating from the traces of γ -matrices read

$$\begin{aligned}
I_{422\mathbf{q}trABbd} &= -\text{tr} \left(\text{diagram}_1 \right) = -2(I_{422\mathbf{q}ABbd} - I_{422\mathbf{q}AbBd} + I_{422\mathbf{q}AdBb}) \\
&= \frac{1}{(8\pi)^4} \left(-\frac{1}{\varepsilon^2} + \frac{1}{\varepsilon} \left(4 - \frac{2}{3}\pi^2 \right) \right), \\
I_{422\mathbf{q}trABCD} &= \text{tr} \left(\text{diagram}_2 \right) = \frac{1}{(8\pi)^4} \frac{\pi^2}{3\varepsilon}.
\end{aligned} \tag{C.9}$$

There is an interesting relation involving the traces. It reads

$$I_{422\mathbf{q}trABCD} = I_{422\mathbf{q}trABbd} + 2I_4 + 4I_{42\mathbf{b}bd} = \frac{1}{(8\pi)^4} \frac{\pi^2}{3\varepsilon}. \tag{C.10}$$

C.2 Integrals with IR divergences

In this subsection we collect the integrals having poles in ε which are due to IR divergences. By suffixes IR and UVIR we thereby label integrals which have one or both IR and UV divergences.

The simplest two-loop integral with both an IR and an UV divergence is the logarithmically divergent tadpole

$$I_{2\text{tp}} = I_{2\text{UVIR}} = \underbrace{\text{tadpole}} = 0. \quad (\text{C.11})$$

It is zero in dimensional regularization, i.e. the IR and the UV divergence cancel against each other. The UV divergence can be extracted by reshuffling the external momentum. In particular, the UV divergence of $I_{2\text{tp}}$ is I_2 defined in (C.2); then the IR divergence of $I_{2\text{tp}}$ is $-I_2$.

The simplest two-loop integral with only an IR divergence is given by

$$I_{2\text{IR}} = \text{triangle} = G(1, 1)G(2 - \lambda, 1) = \frac{1}{(8\pi)^2} \left(-\frac{1}{\varepsilon} + 2(1 + \gamma - \ln 4\pi) + O(\varepsilon) \right). \quad (\text{C.12})$$

One four-loop integral with both, an IR and a UV divergence is given by⁷

$$\begin{aligned} I_{4\text{UVIR}} &= \text{four-loop} = K(G(1, 1)^2 G(1 - \lambda, 1) G(1 - 2\lambda, 2 - \lambda)) \\ &= \frac{1}{(8\pi)^4} \left(-\frac{1}{2\varepsilon^2} + \frac{2}{\varepsilon}(-2 + \gamma - \ln 4\pi) \right). \end{aligned} \quad (\text{C.13})$$

Its IR divergence is extracted as

$$I_{4\text{UVIR}} - I_4 = \frac{1}{(8\pi)^4} \left(\frac{2}{\varepsilon}(-3 + \gamma - \ln 4\pi) \right), \quad (\text{C.14})$$

where I_4 removes the overall UV divergence, since $I_{4\text{UVIR}}$ does not have a UV subdivergence.

The simplest four-loop integral with only an IR divergence as overall divergence is given by

$$\begin{aligned} I_{4\text{IR}} &= \text{four-loop} = K(G(1, 1)^2 G(1 - \lambda, 1) G(2 - 2\lambda, 2 - \lambda)) - K(I_2)I_{2\text{IR}} \\ &= \frac{1}{(8\pi)^4} \left(\frac{2}{\varepsilon}(-3 + \gamma - \ln 4\pi) \right). \end{aligned} \quad (\text{C.15})$$

Here we have subtracted the UV subdivergence.

⁷Note that, according to [15], with $K()$ we mean the extraction of the pole parts of a function of ε .

D Relevant one- and two-loop subdiagrams

In this appendix we collect the results for the planar contributions to the one-loop vector superfield two-point function and the chiral superfield two-loop contributions to the two and four-point functions. The two-point functions have been first computed in [39, 53, 54] in the Landau gauge. Such analysis has been extended to general gauges in [31] where the four point functions have also first been given for the ABJM case. Here we give the results extended to the $U(M) \times U(N)$ ABJ case in the Landau gauge. The two-loop corrections to the chiral propagator and superpotential enter as subdiagrams in the evaluation of the dilatation operator given in section 3.

D.1 One-loop vector two-point function

For the $U(M)$ vector superfield V the one-loop two-point function gets contributions from three kind of diagrams respectively having matter, ghosts and vector superfields propagating in the one-loop bubble.

The contribution coming from the chiral matter superfields is

$$\Sigma_{V,\text{matter}} = \text{---} \circ \text{---} \rightarrow 2N \delta^{ab} G(1, 1) D^\alpha \bar{D}^2 D_\alpha . \quad (\text{D.1})$$

The ghosts correction is

$$\Sigma_{V,\text{ghosts}} = \text{---} \text{---} \rightarrow \frac{1}{2} M \delta^{ab} G(1, 1) (- D^\alpha \bar{D}^2 D_\alpha + \{D^2, \bar{D}^2\}) . \quad (\text{D.2})$$

The diagrams involving a loop of vectors sum up to the following contribution

$$\Sigma_{V,\text{vectors}} = \text{---} \text{---} \rightarrow \frac{1}{2} M \delta^{ab} G(1, 1) (- \{D^2, \bar{D}^2\}) . \quad (\text{D.3})$$

The total contribution to the two-point function for the V superfield is then

$$\Sigma_V = \text{---} \bullet \text{---} \rightarrow \frac{1}{2} \delta^{ab} G(1, 1) (4N - M) D^\alpha \bar{D}^2 D_\alpha . \quad (\text{D.4})$$

The corrections to the $U(N)$ gauge vector \hat{V} two point function are clearly the same with the only difference that one has to exchange M with N in the results.

D.2 Two-loop chiral two-point function

The non-vanishing contributions to the two-point function of chiral superfields can be seen to arise from the following diagrams

$$\begin{aligned}
 & \text{---} \bigcirc \text{---} \rightarrow 2MN I_2 , \\
 & \text{---} \text{---} \text{---} \rightarrow 2MN I_2 , \\
 & \text{---} \text{---} \text{---} \rightarrow -\frac{1}{2} M^2 I_2 , \\
 & \text{---} \text{---} \text{---} \rightarrow -MN(G(1, 1))^2 , \\
 & \text{---} \bullet \text{---} \rightarrow (4N - M)MG(1, 1)G_1(1, 2 - \lambda) \\
 & \qquad \qquad \qquad = \frac{1}{2}(4N - M)M(I_{2\text{tp}} - I_2 + I_{2\text{IR}}) \\
 & \text{---} \bullet \text{---} \rightarrow -\frac{1}{2}(4N - M)MI_{2\text{tp}} ,
 \end{aligned} \tag{D.5}$$

where, in each contribution, we have omitted a factor $D^2 \bar{D}^2$ together with the colour and flavour structures. As discussed in section C.2, the tadpole integral $I_{2\text{tp}}$ is zero in dimensional regularization. However, we keep track of it by splitting its UV and IR divergent parts. This is necessary for the check of the cancellation of the IR divergences performed in appendix E.

Taking into account reflections of the diagrams at the vertical and horizontal axes where necessary, and summing up the contributions, the result reads

$$\Sigma_C = \text{---} \bullet \text{---} \rightarrow -2MN(G(1, 1))^2 + \frac{1}{2}(8MN - (M^2 + N^2))I_{2\text{IR}} . \tag{D.6}$$

Note that the result is UV finite and it includes an IR divergent term which turns out to be gauge dependent [31] and, according to the discussion in appendix E, does not contribute to the dilatation operator.

D.3 Two-loop chiral four-point function

The two-loop renormalization of the superpotential has been studied in [31]. Here we summarize the results and extend them to the ABJ $U(M) \times U(N)$ case. It holds

$$\begin{aligned}
 & \text{Bubble diagram} \rightarrow -(4\pi)^2 \lambda^2 (p_1 + p_2)^2 \text{Bubble diagram} , \\
 & \text{Tadpole diagram} \rightarrow \frac{(4\pi)^2 \lambda^2}{2} (p_1 + p_2)^2 \text{Tadpole diagram} , \\
 & \text{Tadpole diagram} \rightarrow -\frac{(4\pi)^2 \lambda^2}{2} \left(\text{tr}(\gamma^\mu \gamma^\nu \gamma^\alpha \gamma^\beta) \text{Diagram 1} + 2p_2^2 \text{Diagram 2} \right) , \quad (\text{D.7}) \\
 & \text{Tadpole diagram} \rightarrow (4\pi)^2 \lambda \hat{\lambda} \text{tr}(\gamma^\mu \gamma^\nu \gamma^\alpha \gamma^\beta) \text{Diagram 3} , \\
 & \text{Tadpole diagram} \rightarrow (4\pi)^2 \lambda \hat{\lambda} \text{tr}(\gamma^\mu \gamma^\nu \gamma^\rho \gamma^\alpha \gamma^\beta \gamma^\gamma) \text{Diagram 4} .
 \end{aligned}$$

Here the external momenta (p_1, \dots, p_4) are ordered counterclockwise with p_1 the momentum of the upper-left leg.

The last contribution is rather complicated. However, it can be simplified by using momentum conservation to eliminate p_2^ν in the trace and the symmetrization inside the trace as

$$\begin{aligned}
 & \frac{1}{2} (\text{tr}(\gamma^\mu \gamma^\nu \gamma^\rho \gamma^\alpha \gamma^\beta \gamma^\gamma) + \text{tr}(\gamma^\rho \gamma^\nu \gamma^\mu \gamma^\alpha \gamma^\beta \gamma^\gamma)) \\
 & = -g^{\mu\nu} \text{tr}(\gamma^\rho \gamma^\alpha \gamma^\beta \gamma^\gamma) + g^{\mu\rho} \text{tr}(\gamma^\nu \gamma^\alpha \gamma^\beta \gamma^\gamma) - g^{\nu\rho} \text{tr}(\gamma^\mu \gamma^\alpha \gamma^\beta \gamma^\gamma) .
 \end{aligned} \quad (\text{D.8})$$

One then obtains

$$\begin{aligned}
& \text{tr}(\gamma^\mu \gamma^\nu \gamma^\rho \gamma^\alpha \gamma^\beta \gamma^\gamma) \\
&= \text{tr}(\gamma^\rho \gamma^\alpha \gamma^\beta \gamma^\gamma) \left(p_1^2 \left(\text{diagram 1} + \text{diagram 2} + 2 \text{diagram 3} - \text{diagram 4} \right) \right. \\
&= \text{tr}(\gamma^\rho \gamma^\alpha \gamma^\beta \gamma^\gamma) \left(\text{diagram 5} + \text{diagram 6} - \text{diagram 7} \right),
\end{aligned} \tag{D.9}$$

where we have used

$$p_1^2(k-p_1)^\gamma + 2p_1 \cdot (k-p_1)(k-p_1)^\gamma - (k-p_1)^2 p_1^\gamma = k^2(k-p_1)^\gamma - (k-p_1)^2 k^\gamma, \tag{D.10}$$

with k being one of the loop momenta.

The contribution involving the one-loop vacuum polarization reads

$$\begin{aligned}
& \text{diagram 8} \rightarrow (4\pi)^2 \frac{1}{2} (4\lambda \hat{\lambda} - \lambda^2) \\
& \left(-(p_1 + p_2)^2 \text{diagram 9} + p_1^2 \text{diagram 10} + p_2^2 \text{diagram 11} \right).
\end{aligned} \tag{D.11}$$

Considering a factor -1 from the cancellation of the propagator connecting the chiral vertex to the two-loop self energy, we obtain from the D-algebra manipulations

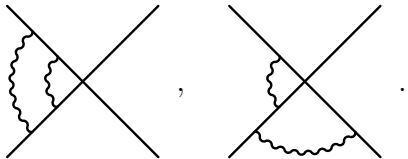
$$\text{diagram 12} \rightarrow (4\pi)^2 \left(2\lambda \hat{\lambda} p_1^2 \text{diagram 13} - \frac{1}{2} (8\lambda \hat{\lambda} - (\lambda^2 + \hat{\lambda}^2)) p_1^2 \text{diagram 14} \right). \tag{D.12}$$

Let us conclude by mentioning a useful property that was used in appendix E. In the combination

$$\text{diagram 15} + \frac{1}{2} \left(\text{diagram 16} + \text{diagram 17} \right) \tag{D.13}$$

the infrared divergence from the integrals involving the first leg is cancelled out.

There are two other diagrams with non-trivial D-algebra and colour structure


(D.14)

Interestingly, these can be seen to be proportional to the very same integrals which appear in components [15]. The two diagrams are zero due to the vanishing of the one-loop triangle subdiagrams.

E Cancellation of IR divergences

In order to check the cancellation of the IR divergences, together with the contributions having both UV and IR divergences given in section 4, we have to include diagrams that have pure IR poles and would have been excluded by the UV finiteness conditions of subsection 4.1. The cancellation of IR divergences in the combination (D.13) means that chiral and anti-chiral vertices with any number of legs and with external propagators are free of IR divergences from perturbative corrections. In the following we will hence attach propagators to the external fields of the diagrams that appear at four loops as quantum corrections of a chiral composite operator. This does not affect the UV poles, since the chiral self-energy is UV finite as demonstrated in appendix D.2.

The contributions to the $\chi(1)$ structure with only an IR divergence are given by

$$\begin{aligned}
V_{r44} &= \begin{array}{c} \text{Diagram: A loop with a wavy line and a vertex} \\ \text{Diagram: A loop with a wavy line and a vertex} \end{array} \rightarrow \frac{(4\pi)^4}{k^4} MN(4MN - M^2) I_{4\text{IR}} \chi(1) \\
&= \frac{\lambda\hat{\lambda}}{16} (4\lambda\hat{\lambda} - \lambda^2) \left(\frac{2}{\varepsilon} (-3 + \gamma - \ln 4\pi) \chi(1) \right), \\
V_{r45} &= \begin{array}{c} \text{Diagram: A loop with a wavy line and a vertex} \\ \text{Diagram: A loop with a wavy line and a vertex} \end{array} \rightarrow -\frac{(4\pi)^4}{k^4} \frac{MN}{2} (4MN - M^2) (I_{4\text{IR}} + I_{4\text{UVIR}} - I_4) \chi(1) \\
&= -\frac{\lambda\hat{\lambda}}{16} (4\lambda\hat{\lambda} - \lambda^2) \left(\frac{2}{\varepsilon} (-3 + \gamma - \ln 4\pi) \chi(1) \right), \\
V_{r46} &= \begin{array}{c} \text{Diagram: A loop with a wavy line and a vertex} \\ \text{Diagram: A loop with a wavy line and a vertex} \end{array} \rightarrow \frac{(4\pi)^4}{k^4} \frac{MN}{2} (4MN - M^2) (I_{4\text{UVIR}} - I_4 + I_2 I_{2\text{IR}} - \text{K}(I_2) I_{2\text{IR}}) \chi(1) \\
&= \frac{\lambda\hat{\lambda}}{16} (4\lambda\hat{\lambda} - \lambda^2) \left(\frac{2}{\varepsilon} (-3 + \gamma - \ln 4\pi) \chi(1) \right), \\
V_{r37} &= \begin{array}{c} \text{Diagram: A loop with a wavy line and a vertex} \\ \text{Diagram: A loop with a wavy line and a vertex} \end{array} \rightarrow -\frac{(4\pi)^4}{k^4} \frac{MN}{2} (4MN - M^2) (I_{4\text{IR}} + I_2 I_{2\text{IR}} - \text{K}(I_2) I_{2\text{IR}}) \chi(1) \\
&= -\frac{\lambda\hat{\lambda}}{16} (4\lambda\hat{\lambda} - \lambda^2) \left(\frac{2}{\varepsilon} (-3 + \gamma - \ln 4\pi) \chi(1) \right), \\
V_{r38} &= \begin{array}{c} \text{Diagram: A loop with a wavy line and a vertex} \\ \text{Diagram: A loop with a wavy line and a vertex} \end{array} \rightarrow -\frac{(4\pi)^4}{k^4} \frac{MN}{2} (4MN - M^2) (I_4 - I_{4\text{UVIR}} - I_2 I_{2\text{IR}} + \text{K}(I_2) I_{2\text{IR}}) \chi(1) \\
&= \frac{\lambda\hat{\lambda}}{16} (4\lambda\hat{\lambda} - \lambda^2) \left(\frac{2}{\varepsilon} (-3 + \gamma - \ln 4\pi) \chi(1) \right).
\end{aligned} \tag{E.1}$$

where we have given only the IR pole terms, and the UV subdivergences have been subtracted.

We also have to consider the correction of the chiral propagator that is a neighbour of the fields interacting via $\chi(1)$

$$\begin{aligned}
V_{r3s} &= \begin{array}{c} \text{Diagram: A loop with a wavy line and a vertex} \\ \text{Diagram: A loop with a wavy line and a vertex} \end{array} \rightarrow -\frac{(4\pi)^4}{k^4} \frac{MN}{2} (8MN - (M^2 + N^2)) (I_2 - \text{K}(I_2)) I_{2\text{IR}} \chi(1) \\
&= -\frac{\lambda\hat{\lambda}}{16} (8\lambda\hat{\lambda} - (\lambda^2 + \hat{\lambda}^2)) \left(\frac{1}{\varepsilon} (-3 + \gamma - \ln 4\pi) \chi(1) \right).
\end{aligned} \tag{E.2}$$

According to (D.13), one half of this contribution has to be taken into account, since the other half should cancel part of the IR divergence from an interaction of the isolated leg via a one-loop corrected gauge propagator with its neighbour to the right. Similar considerations hold also for the reflected diagram of V_{r3s} , such that the total contribution of these diagrams to the IR divergence is $\frac{1}{2}(1 + \mathcal{R})V_{r3s}$.

Further IR divergent contributions from self energy corrections of the three external and one internal line at the upper chiral vertex that forms $\chi(1)$ cancel among respective diagrams in which two of these lines are interacting via one-loop corrected gauge prop-

agator. This is guaranteed by (D.13) since in the considered propagators are attached to their external lines.

At this point a simple way to check the cancellation of the IR divergences is to sum up all the contribution containing them and check that the result is the same as if from the very beginning we had omitted all IR divergent diagrams, and had only considered V_{r35}^{UV} and V_{r36}^{UV} . In fact, the sum

$$\begin{aligned}
& - (1 + \mathcal{R})(V_{r35} + V_{r44} + V_{r45} + V_{r46} + V_{r37} + V_{r38}) - 3V_{r36} - \frac{1}{2}(1 + \mathcal{R})V_{r3s} \\
& = \frac{(4\pi)^4}{k^4} MN \left(-6MNI_{4\text{bbb}} + \frac{1}{2}(8MN - (M^2 + N^2))(3I_4 + 2I_{42\text{bbd}}) \right) \chi(1) \quad (\text{E.3}) \\
& = \frac{\lambda\hat{\lambda}}{16} \left(-\lambda\hat{\lambda}\frac{3\pi^2}{\varepsilon} + (8\lambda\hat{\lambda} - (\lambda^2 + \hat{\lambda}^2)) \left(-\frac{1}{4\varepsilon^2} + \frac{1}{\varepsilon} \left(1 + \frac{\pi^2}{4} \right) \right) \right) \chi(1)
\end{aligned}$$

turns out to be equal to

$$- (1 + \mathcal{R})V_{r35}^{\text{UV}} - 3V_{r36}^{\text{UV}} , \quad (\text{E.4})$$

which is the respective contribution of only the overall UV divergences from the diagrams with also an IR divergence to (4.10).

It is important to note that, besides the previously described check of the cancellation of the IR divergences, we have also performed the full computation of the range three contribution in the IR-safe η -gauge described in [31]. The result turns out to be the same.

F Double poles

In this appendix we check explicitly the cancellation of the double poles in $\ln \mathcal{Z}$. For that we need to consider diagrams which are responsible for interactions between magnons at odd and even sites which are proportional to chiral functions $\chi(1, 2)$ and $\chi(2, 3)$. We start by computing those contributions, and then we prove the complete cancellation of the double poles.

F.1 Odd- and even-site magnon interactions

The relevant diagrams that couple the odd and even site magnons with each other are the following ones

$$\begin{aligned}
S_{\text{mixed}} &= \begin{array}{c} \text{Diagram 1: A diagram with two vertices connected by a wavy line, with external lines forming a loop structure.} \end{array} \rightarrow \frac{(4\pi)^4}{k^4} (MN)^2 I_4 \chi(1, 2) = \frac{(\lambda\hat{\lambda})^2}{16} \left(-\frac{1}{2\varepsilon^2} + \frac{2}{\varepsilon} \right) \chi(1, 2) , \\
V_{\text{mixed1}} &= \begin{array}{c} \text{Diagram 2: A diagram with two vertices connected by a wavy line, with external lines forming a loop structure.} \end{array} \rightarrow \frac{(4\pi)^4}{k^4} (MN)^2 I_{42\text{bb0cd}} \chi(1, 2) = \frac{(\lambda\hat{\lambda})^2}{16} \left(\frac{1}{4\varepsilon^2} - \frac{3}{2\varepsilon} \right) \chi(1, 2) , \\
V_{\text{mixed2}} &= \begin{array}{c} \text{Diagram 3: A diagram with two vertices connected by a wavy line, with external lines forming a loop structure.} \end{array} \rightarrow -\frac{(4\pi)^4}{k^4} \frac{(MN)^2}{2} I_{422\text{btrABcd}} \chi(1, 2) = \frac{(\lambda\hat{\lambda})^2}{16} \left(-\frac{1}{2\varepsilon^2} + \frac{1}{\varepsilon} \right) \chi(1, 2) . \quad (\text{F.1})
\end{aligned}$$

In the sum of all contributions one has to consider the reflected diagrams. The second contribution acquires an additional factor of two due to two distinct positions for the vector vertices which are not mapped to each other under reflection. The result for the mixed renormalization constant reads⁸

$$\mathcal{Z}_{4,\text{mixed}} = -(1 + \mathcal{R})(S_{\text{mixed}} + 2V_{\text{mixed}1} + V_{\text{mixed}2}) = \frac{(\lambda\hat{\lambda})^2}{16} \frac{1}{\varepsilon^2} \chi(1, 2) . \quad (\text{F.2})$$

As expected [55], the $1/\varepsilon$ pole is cancelled out such that at four loops there is no contribution to the dilatation operator that couples the magnons at odd and even sites.

F.2 Double pole cancellation

Summing up the contributions to the $1/\varepsilon^2$ poles of the odd-site sector to the four-loop \mathcal{Z} from (4.4), (4.6), (4.10) and (F.2), we obtain

$$\begin{aligned} \bar{\lambda}^4(\mathcal{Z}_{4,\text{odd}} + \mathcal{Z}_{4,\text{mixed}})|_{\frac{1}{\varepsilon^2}} &= (\mathcal{Z}_{r5,\text{odd}} + \mathcal{Z}_{4,\text{mixed}} + \mathcal{Z}_{r4,\text{odd}} + \mathcal{Z}_{r3,\text{odd}})|_{\frac{1}{\varepsilon^2}} \\ &= \frac{\bar{\lambda}^4}{16\varepsilon^2} \left[\frac{1}{2}(\chi(1, 3) + \chi(3, 1)) + \chi(1, 2) - \chi(1) \right] . \end{aligned} \quad (\text{F.3})$$

In the definition of the dilatation operator, the logarithm guarantees that all higher order poles in ε cancel out, such that $\ln \mathcal{Z}$ only contains simple $\frac{1}{\varepsilon}$ poles. Inserting (3.2), the expansion reads

$$\ln \mathcal{Z} = \bar{\lambda}^2 \mathcal{Z}_2 + \bar{\lambda}^4 \left(\mathcal{Z}_4 - \frac{1}{2} \mathcal{Z}_2^2 \right) + \mathcal{O}(\bar{\lambda}^6) . \quad (\text{F.4})$$

Let us now check the double pole cancellations in the $\bar{\lambda}^4$ term. The two-loop contribution to the renormalization constant for operators of length L can be written as

$$\bar{\lambda}^2 \mathcal{Z}_2 = - \sum_{i=1}^{2L} \text{Diagram}_i = - \frac{\lambda\hat{\lambda}}{4} \frac{1}{\varepsilon} (\chi(1) + \chi(2)) , \quad (\text{F.5})$$

where we have indicated the sum over the sites explicitly. It has an obvious decomposition into two parts acting exclusively on even and on odd sites, respectively. The square of the above result can be decomposed as follows

$$\frac{1}{2} \mathcal{Z}_2^2 = \mathcal{Z}_{22,\text{dc}} + \mathcal{Z}_{22,\text{S}} . \quad (\text{F.6})$$

⁸There is another contribution with identical prefactor that involves the chiral function $\chi(2, 3)$ that we associate to the even site sector.

The individual terms are given by

$$\begin{aligned}
\bar{\lambda}^4 \mathcal{Z}_{22,\text{dc}} &= \sum_{j \geq i+3}^{2L} \left(\text{diagram}_i \text{diagram}_j \right) \\
\bar{\lambda}^4 \mathcal{Z}_{22,S} &= \frac{1}{2} \sum_{i=1}^{2L} \left(\text{diagram}_i^{(1)} + \text{diagram}_i^{(2)} + \text{diagram}_i^{(3)} + \text{diagram}_i^{(4)} + \text{diagram}_i^{(5)} \right) \quad (\text{F.7}) \\
&\rightarrow \frac{1}{2} \frac{(4\pi)^4}{k^4} M^2 N^2 K(I_2)^2 (\chi(1,3) + \chi(3,1) + 2\chi(1,2) - 2\chi(1)) \\
&= \frac{(\lambda \hat{\lambda})^2}{16} \frac{1}{2\varepsilon^2} (\chi(1,3) + \chi(3,1) + 2\chi(1,2) - 2\chi(1)) ,
\end{aligned}$$

where the arrow denotes that in the final result we have considered the chiral functions with odd indices only and $\chi(1,2)$ and neglected the ones with only even indices and $\chi(2,3)$.

According to (F.6), the square of the two-loop contribution expands as

$$\frac{1}{2} (\bar{\lambda} \mathcal{Z}_2)^2 = \frac{(\lambda \hat{\lambda})^2}{16} \frac{1}{2\varepsilon^2} (\chi(1,3) + \chi(3,1) + 2\chi(1,2) - 2\chi(1)) + \dots , \quad (\text{F.8})$$

where we have neglected the chiral functions with only even arguments and $\chi(2,3)$. We have also disregarded the terms $\mathcal{Z}_{22,\text{dc}}$ which trivially cancel against four-loop diagrams that only contain double poles and hence become disconnected when the composite operator is removed. We have omitted to present these diagrams in the paper.

Comparing equations (F.3) and (F.8) we finally find our desired result

$$\left(\mathcal{Z}_4 - \frac{1}{2} \mathcal{Z}_2^2 \right) \Big|_{\frac{1}{\varepsilon^2}} = 0 , \quad (\text{F.9})$$

where we have considered that the discussion is identical for the neglected contributions with chiral functions with even arguments and $\chi(2,3)$.

References

- [1] O. Aharony, O. Bergman, D. L. Jafferis, and J. Maldacena, $\mathcal{N} = 6$ superconformal Chern-Simons-matter theories, M2-branes and their gravity duals, [arXiv:0806.1218](#).
- [2] J. A. Minahan and K. Zarembo, *The Bethe ansatz for superconformal Chern-Simons*, *JHEP* **09** (2008) 040, [[arXiv:0806.3951](#)].
- [3] D. Gaiotto, S. Giombi, and X. Yin, *Spin Chains in $\mathcal{N} = 6$ Superconformal Chern-Simons-Matter Theory*, *JHEP* **04** (2009) 066, [[arXiv:0806.4589](#)].
- [4] D. Bak and S.-J. Rey, *Integrable Spin Chain in Superconformal Chern-Simons Theory*, *JHEP* **10** (2008) 053, [[arXiv:0807.2063](#)].
- [5] N. Gromov and P. Vieira, *The all loop AdS₄/CFT₃ Bethe ansatz*, *JHEP* **01** (2009) 016, [[arXiv:0807.0777](#)].
- [6] N. Gromov, V. Kazakov, and P. Vieira, *Exact Spectrum of Planar $\mathcal{N} = 4$ Supersymmetric Yang-Mills Theory: Konishi Dimension at Any Coupling*, *Phys. Rev. Lett.* **104** (2010) 211601, [[arXiv:0906.4240](#)].

- [7] S. Frolov, *Konishi operator at intermediate coupling*, [arXiv:1006.5032](#).
- [8] O. Aharony, O. Bergman, and D. L. Jafferis, *Fractional M2-branes*, *JHEP* **11** (2008) 043, [[arXiv:0807.4924](#)].
- [9] B. I. Zwiebel, *Two-loop Integrability of Planar $\mathcal{N} = 6$ Superconformal Chern-Simons Theory*, *J. Phys.* **A42** (2009) 495402, [[arXiv:0901.0411](#)].
- [10] J. A. Minahan, W. Schulgin, and K. Zarembo, *Two loop integrability for Chern-Simons theories with $\mathcal{N} = 6$ supersymmetry*, *JHEP* **03** (2009) 057, [[arXiv:0901.1142](#)].
- [11] D. Bak, D. Gang, and S.-J. Rey, *Integrable Spin Chain of Superconformal $U(M) \times U(N)$ Chern-Simons Theory*, *JHEP* **10** (2008) 038, [[arXiv:0808.0170](#)].
- [12] T. Nishioka and T. Takayanagi, *On Type IIA Penrose Limit and $\mathcal{N} = 6$ Chern-Simons Theories*, *JHEP* **08** (2008) 001, [[arXiv:0806.3391](#)].
- [13] G. Grignani, T. Harmark, and M. Orselli, *The $SU(2) \times SU(2)$ sector in the string dual of $\mathcal{N} = 6$ superconformal Chern-Simons theory*, *Nucl. Phys.* **B810** (2009) 115–134, [[arXiv:0806.4959](#)].
- [14] J. A. Minahan, O. Ohlsson Sax, and C. Sieg, *Magnon dispersion to four loops in the ABJM and ABJ models*, *J. Phys.* **A43** (2010) 275402, [[arXiv:0908.2463](#)].
- [15] J. A. Minahan, O. Ohlsson Sax, and C. Sieg, *Anomalous dimensions at four loops in $\mathcal{N} = 6$ superconformal Chern-Simons theories*, [arXiv:0912.3460](#).
- [16] C. Sieg, *Superspace computation of the three-loop dilatation operator of $\mathcal{N} = 4$ SYM theory*, [arXiv:1008.3351](#).
- [17] D. Serban and M. Staudacher, *Planar $\mathcal{N} = 4$ gauge theory and the Inozemtsev long range spin chain*, *JHEP* **06** (2004) 001, [[hep-th/0401057](#)].
- [18] C. Sieg and A. Torrielli, *Wrapping interactions and the genus expansion of the 2-point function of composite operators*, *Nucl. Phys.* **B723** (2005) 3–32, [[hep-th/0505071](#)].
- [19] F. Fiamberti, A. Santambrogio, C. Sieg, and D. Zanon, *Anomalous dimension with wrapping at four loops in $\mathcal{N} = 4$ SYM*, *Nucl. Phys.* **B805** (2008) 231–266, [[arXiv:0806.2095](#)].
- [20] F. Fiamberti, A. Santambrogio, and C. Sieg, *Five-loop anomalous dimension at critical wrapping order in $\mathcal{N} = 4$ SYM*, *JHEP* **03** (2010) 103, [[arXiv:0908.0234](#)].
- [21] A. Mauri, S. Penati, A. Santambrogio, and D. Zanon, *Exact results in planar $N = 1$ superconformal Yang-Mills theory*, *JHEP* **11** (2005) 024, [[hep-th/0507282](#)].
- [22] F. Fiamberti, A. Santambrogio, C. Sieg, and D. Zanon, *Finite-size effects in the superconformal beta-deformed $\mathcal{N} = 4$ SYM*, *JHEP* **08** (2008) 057, [[arXiv:0806.2103](#)].
- [23] F. Fiamberti, A. Santambrogio, C. Sieg, and D. Zanon, *Single impurity operators at critical wrapping order in the beta-deformed $\mathcal{N} = 4$ SYM*, *JHEP* **08** (2009) 034, [[arXiv:0811.4594](#)].
- [24] T. McLoughlin, R. Roiban, and A. A. Tseytlin, *Quantum spinning strings in $AdS_4 \times CP^3$: testing the Bethe Ansatz proposal*, *JHEP* **11** (2008) 069, [[arXiv:0809.4038](#)].
- [25] N. Gromov and V. Mikhaylov, *Comment on the Scaling Function in $AdS_4 \times CP^3$* , *JHEP* **04** (2009) 083, [[arXiv:0807.4897](#)].
- [26] A. Kapustin, B. Willett, and I. Yaakov, *Exact Results for Wilson Loops in Superconformal Chern-Simons Theories with Matter*, *JHEP* **03** (2010) 089, [[arXiv:0909.4559](#)].
- [27] N. Drukker and D. Trancanelli, *A supermatrix model for $\mathcal{N} = 6$ super Chern-Simons-matter theory*, *JHEP* **02** (2010) 058, [[arXiv:0912.3006](#)].
- [28] M. Marino and P. Putrov, *Exact Results in ABJM Theory from Topological Strings*, *JHEP* **06** (2010) 011, [[arXiv:0912.3074](#)].
- [29] N. Drukker, M. Marino, and P. Putrov, *From weak to strong coupling in ABJM theory*, [arXiv:1007.3837](#).

- [30] M. Benna, I. Klebanov, T. Klose, and M. Smedback, *Superconformal Chern-Simons Theories and AdS_4/CFT_3 Correspondence*, *JHEP* **09** (2008) 072, [[arXiv:0806.1519](#)].
- [31] M. Leoni and A. Mauri, *On the infrared behaviour of 3d Chern-Simons theories in $\mathcal{N} = 2$ superspace*, [arXiv:1006.2341](#).
- [32] S. J. Gates, M. T. Grisaru, M. Rocek, and W. Siegel, *Superspace, or one thousand and one lessons in supersymmetry*, *Front. Phys.* **58** (1983) 1–548, [[hep-th/0108200](#)].
- [33] B. M. Zupnik and D. G. Pak, *Superfield formulation of the simplest three-dimensional gauge theories and conformal supergravities*, *Theor. Math. Phys.* **77** (1988) 1070–1076.
- [34] E. A. Ivanov, *Chern-Simons matter systems with manifest $N=2$ supersymmetry*, *Phys. Lett.* **B268** (1991) 203–208.
- [35] S. J. Gates, Jr. and H. Nishino, *Remarks on the $N=2$ supersymmetric Chern-Simons theories*, *Phys. Lett.* **B281** (1992) 72–80.
- [36] H. Nishino and S. J. Gates, Jr., *Chern-Simons theories with supersymmetries in three-dimensions*, *Int. J. Mod. Phys.* **A8** (1993) 3371–3422.
- [37] L. V. Avdeev, G. V. Grigorev, and D. I. Kazakov, *Renormalizations in Abelian Chern-Simons field theories with matter*, *Nucl. Phys.* **B382** (1992) 561–580.
- [38] L. V. Avdeev, D. I. Kazakov, and I. N. Kondrashuk, *Renormalizations in supersymmetric and nonsupersymmetric nonAbelian Chern-Simons field theories with matter*, *Nucl. Phys.* **B391** (1993) 333–357.
- [39] M. S. Bianchi, S. Penati, and M. Siani, *Infrared stability of ABJ-like theories*, *JHEP* **01** (2010) 080, [[arXiv:0910.5200](#)].
- [40] L. F. Abbott, M. T. Grisaru, and D. Zanon, *Infrared divergences and a nonlocal gauge for superspace Yang-Mills theory*, *Nucl. Phys.* **B244** (1984) 454.
- [41] T. McLoughlin and R. Roiban, *Spinning strings at one-loop in $AdS_4 \times P^3$* , *JHEP* **12** (2008) 101, [[arXiv:0807.3965](#)].
- [42] L. F. Alday, G. Arutyunov, and D. Bykov, *Semiclassical Quantization of Spinning Strings in $AdS_4 \times CP^3$* , *JHEP* **11** (2008) 089, [[arXiv:0807.4400](#)].
- [43] C. Krishnan, *AdS_4/CFT_3 at One Loop*, *JHEP* **09** (2008) 092, [[arXiv:0807.4561](#)].
- [44] V. Mikhailov, *On the Fermionic Frequencies of Circular Strings*, *J. Phys.* **A43** (2010) 335401, [[arXiv:1002.1831](#)].
- [45] M. C. Abbott, I. Aniceto, and D. Bombardelli, *Quantum Strings and the AdS_4/CFT_3 Interpolating Function*, [arXiv:1006.2174](#).
- [46] I. Shenderovich, *Giant magnons in AdS_4/CFT_3 : dispersion, quantization and finite-size corrections*, [arXiv:0807.2861](#).
- [47] D. Astolfi, V. G. M. Puletti, G. Grignani, T. Harmark, and M. Orselli, *Finite-size corrections in the $SU(2) \times SU(2)$ sector of type IIA string theory on $AdS_4 \times CP^3$* , *Nucl. Phys.* **B810** (2009) 150–173, [[arXiv:0807.1527](#)].
- [48] J. A. Minahan, O. Ohlsson Sax, and C. Sieg, *A limit on the ABJ model*, [arXiv:1005.1786](#).
- [49] N. A. Nekrasov, *Seiberg-Witten Prepotential From Instanton Counting*, *Adv. Theor. Math. Phys.* **7** (2004) 831–864, [[hep-th/0206161](#)].
- [50] V. Pestun, *Localization of gauge theory on a four-sphere and supersymmetric Wilson loops*, [arXiv:0712.2824](#).
- [51] M. Marino, *Chern-Simons theory, matrix integrals, and perturbative three-manifold invariants*, *Commun. Math. Phys.* **253** (2004) 25–49, [[hep-th/0207096](#)].
- [52] N. Halmagyi and V. Yasnov, *The spectral curve of the Lens space matrix model*, *JHEP* **11** (2009) 104, [[hep-th/0311117](#)].

- [53] N. Akerblom, C. Saemann, and M. Wolf, *Marginal Deformations and 3-Algebra Structures*, *Nucl. Phys.* **B826** (2010) 456–489, [[arXiv:0906.1705](#)].
- [54] M. S. Bianchi, S. Penati, and M. Siani, *Infrared Stability of $\mathcal{N} = 2$ Chern-Simons Matter Theories*, *JHEP* **05** (2010) 106, [[arXiv:0912.4282](#)].
- [55] D. Bak, H. Min, and S.-J. Rey, *Generalized Dynamical Spin Chain and 4-Loop Integrability in $\mathcal{N} = 6$ Superconformal Chern-Simons Theory*, *Nucl. Phys.* **B827** (2010) 381–405, [[arXiv:0904.4677](#)].